

1 **Global combustion sources of organic aerosols: Model comparison**  
2 **with 84 AMS factor analysis data sets**

3

4 **Tsimpidi A.P.<sup>1</sup>, Karydis V.A.<sup>1</sup>, Pandis S.N.<sup>2,3</sup> and Lelieveld J.<sup>1,4</sup>**

5

6 <sup>1</sup> Max Planck Institute for Chemistry, Mainz, Germany

7

<sup>2</sup> Department of Chemical Engineering, University of Patras, Patras, Greece

8

<sup>3</sup> Department of Chemical Engineering, Carnegie Mellon University, Pittsburgh, PA, USA

9

<sup>4</sup> Energy, Environment and Water Research Center, Cyprus Institute, Nicosia, Cyprus

10

\*Corresponding author e-mail: [a.tsimpidi@mpic.de](mailto:a.tsimpidi@mpic.de)

11

## 12 **Abstract**

13 Emissions of organic compounds from biomass, biofuel and fossil fuel combustion  
14 strongly influence the global atmospheric aerosol load. Some of the organics are  
15 directly released as primary organic aerosol (POA). Most are emitted in the gas phase  
16 and undergo chemical transformations (i.e., oxidation by hydroxyl radical) and form  
17 secondary organic aerosol (SOA). In this work we use the global chemistry climate  
18 model EMAC with a computationally efficient module for the description of organic  
19 aerosol (OA) composition and evolution in the atmosphere (ORACLE). The  
20 tropospheric burden of open biomass and anthropogenic (fossil and biofuel)  
21 combustion particles is estimated to be 0.59 Tg and 0.63 Tg, respectively, accounting  
22 for about 30% and 32% of the total tropospheric OA load. About 30% of the open  
23 biomass burning and 10% of the anthropogenic combustion aerosols originate from  
24 direct particle emissions while the rest is formed in the atmosphere. A comprehensive  
25 dataset of aerosol mass spectrometer (AMS) measurements along with factor-analysis  
26 results from 84 field campaigns across the Northern Hemisphere are used to evaluate  
27 the model results. Both the AMS observations and the model results suggest that over  
28 urban areas both POA (25-40%) and SOA (60-75%) contribute substantially to the  
29 overall OA mass while further downwind and in rural areas the POA concentrations  
30 decrease substantially and SOA dominates (80-85%). EMAC does a reasonable job in  
31 reproducing POA and SOA levels during most of the year. However, it tends to  
32 underpredict POA and SOA concentrations during winter indicating that the model  
33 misses wintertime sources of OA (e.g., residential biofuel use) and SOA formation  
34 pathways (e.g., multiphase oxidation).

35

## 36 **1. Introduction**

37

38 Organic aerosol (OA) is a major contributor to fine particulate matter mass with  
39 potentially harmful effects on the environment and human health (Lelieveld et al.,  
40 2013; Poschl, 2005), however, the sources are poorly understood (Kanakidou et al.,  
41 2005; Goldstein and Galbally, 2007; Donahue et al., 2009; Tsigaridis et al., 2014). OA  
42 comprises primary organic aerosol (POA), i.e., directly emitted in the particulate  
43 phase, and secondary organic aerosol (SOA), formed within the atmosphere from the  
44 oxidation of gas-phase precursors. POA constitutes the particulate OA fraction

45 emitted by anthropogenic combustion processes (i.e., fossil fuels, biofuels) and open  
46 biomass burning (i.e., savanna and forest fires). Anthropogenic combustion emissions  
47 of particulate organic carbon (OC) are estimated at 13.9 Tg C yr<sup>-1</sup> for the year 2005  
48 (Clarke et al., 2007). OC emissions from open biomass burning range from 13.5 Tg C  
49 yr<sup>-1</sup> to 21.4 Tg C yr<sup>-1</sup> during the decade since 2000 (Van der Werf et al., 2010). POA  
50 emitted from combustion sources can evaporate rapidly during atmospheric dilution  
51 depending on ambient concentrations (Robinson et al., 2010; Ranjan et al., 2012; May  
52 et al., 2014). The phase partitioning of the emitted POA depends on the volatility  
53 distribution of the emissions. This distribution includes low volatility (LVOC;  $C^* <$   
54  $0.32 \mu\text{g m}^{-3}$ ), semivolatile (SVOC;  $0.32 \mu\text{g m}^{-3} < C^* < 320 \mu\text{g m}^{-3}$ ), and intermediate  
55 volatility (IVOC;  $3.2 \times 10^2 \mu\text{g m}^{-3} < C^* < 3.2 \times 10^6 \mu\text{g m}^{-3}$ ) organic compounds. The  
56 corresponding emission factors can be measured using dilution samplers and are  
57 estimated as a function of the saturation concentration of the emitted organic  
58 compounds (Grieshop et al., 2009). Traditional emission inventories (e.g., Clarke et  
59 al., 2007; Van Der Werf et al., 2010) account only for a small fraction of the emitted  
60 IVOCs since they are based on filter samples collected at aerosol concentrations up to  
61  $10^4 \mu\text{g m}^{-3}$  (Shrivastava et al., 2008; Robinson et al., 2010). The amount of IVOC  
62 emissions missing in traditional inventories is estimated to be between 0.25 and 2.8  
63 times POA emissions, depending on the type of the source (Shrivastava et al., 2008;  
64 Robinson et al., 2010).

65 Organic emissions further downwind mix with background air, resulting in cooling  
66 and dilution and altering the gas-particle partitioning. The organic compounds that  
67 remain in the gas phase can undergo chemical transformations (i.e., oxidation by  
68 hydroxyl radical), become less volatile and may be transferred into SOA (Donahue et  
69 al., 2006). Therefore, in addition to direct emissions of POA, it is important to  
70 understand the potential of combustion emissions to contribute to SOA formation.  
71 Numerous studies have indicated that SOA usually exceeds POA even in urban  
72 environments with substantial primary emissions (Jimenez et al., 2009; Stone et al.,  
73 2009; Sun et al., 2011; Mohr et al., 2012; Hayes et al., 2013). However, the overall  
74 contribution of combustion emissions to ambient SOA and OA remains uncertain  
75 (Chirico et al., 2010; Miracolo et al., 2011; Samy and Zielinska, 2010; Gentner et al.,  
76 2012; Bahreini et al., 2012; Gordon et al., 2014). Together with the OA mass  
77 concentration, the hygroscopic, chemical and optical properties continue to change

78 because of chemical processing by gas-phase oxidants (Jimenez et al., 2009). These  
79 changes affect the OA radiative forcing on climate by direct and indirect effects, the  
80 latter through cloud formation (Poschl, 2005; McFiggans et al., 2006; IPCC; 2013).

81 Mass spectrometry has been widely used in aerosol analyses because of the  
82 universal, sensitive and rapid detection of aerosol components (Suess and Prather,  
83 1999). The Aerosol Mass Spectrometer (AMS) (Jimenez et al., 2003) has been the  
84 most commonly used instrument in recent years. AMS is capable of quantitatively  
85 measuring the OA mass concentrations with high time and particle size resolution  
86 (Takegawa et al., 2005; Zhang et al., 2005b). Several factor analysis techniques have  
87 been employed to extract information about processes and sources of OA. These  
88 techniques include principal component analysis (CPCA; Zhang et al., 2005a),  
89 multiple component analysis (MCA; Zhang et al., 2007), hierarchical cluster analysis  
90 (Marcolli et al., 2006), the Multilinear Engine (ME-2; Lanz et al., 2008), and positive  
91 matrix factorization (PMF; Paatero and Tapper, 1994; Paatero, 1997), with the latter  
92 being the most commonly used (Lanz et al., 2007; Nemitz et al., 2008; Aiken et al.,  
93 2009; Ulbrich et al., 2009; DeCarlo et al., 2010; Mohr et al., 2012; Hayes et al., 2013;  
94 Crippa et al., 2014; Carbone et al., 2014; Chen et al., 2015).

95 PMF allows the classification of OA into several types based on different temporal  
96 and mass spectral signatures. Two major components often resolved by the analysis of  
97 the AMS measurements are hydrocarbon-like organic aerosol (HOA) and oxygenated  
98 organic aerosol (OOA) (Zhang et al., 2007; Jimenez et al., 2009). Biomass burning  
99 OA (BBOA), marine-related OA (MOA) and cooking OA (COA) are other OA  
100 components that PMF may identify as important components of the observed OA  
101 (Lanz et al., 2010; Mohr et al., 2012; Kostenidou et al., 2013; Crippa et al., 2013a).  
102 HOA correlates with combustion tracers (e.g., CO, EC, and NO<sub>x</sub>) and is considered as  
103 a surrogate for fossil fuel combustion POA (Lanz et al., 2007; Ulbrich et al., 2009;  
104 Crippa et al., 2014). BBOA correlates with tracers from biomass burning (e.g.,  
105 acetonitrile, levoglucosan, and potassium) and is considered a surrogate of biomass  
106 burning POA (Aiken et al., 2010; Lanz et al., 2010; Crippa et al., 2014). OOA often  
107 correlates with secondary pollutants (e.g. ozone, sulfate, and nitrate) and is considered  
108 a surrogate for SOA (Jimenez et al., 2009; Ng et al., 2011; ). However, Crippa et al.  
109 (2014) have reported that the OOA correlation with secondary inorganic species  
110 might not be very high in at least some field campaigns. OOA can include SOA from

111 various precursors, such as anthropogenic and biogenic VOCs, as well as SVOCs and  
112 IVOCs from fossil fuel, biofuel and open biomass burning. PMF often classifies OOA  
113 into two subtypes that differ in the degree of oxidation: a more strongly oxygenated  
114 low-volatility OOA (LV-OOA) often correlating with sulfate, and a less oxygenated  
115 semivolatile OOA (SV-OOA) usually correlating with nitrate (Jimenez et al., 2009;  
116 Crippa et al., 2014). Field campaigns in the Northern Hemisphere have shown that  
117 HOA accounts for approximately one third of the OA in urban sites and OOA  
118 accounts for the remaining two thirds, while OOA represents roughly 95% of the OA  
119 in rural/remote regions (Zhang et al., 2007).

120 Global chemistry climate and chemical transport models systematically  
121 underpredict OA levels, especially over and downwind of anthropogenic source  
122 regions (Tsigaridis et al., 2014). At the same time, global models tend to predict a  
123 dominance of POA at mid-latitudes in the Northern Hemisphere while measurements  
124 indicate the opposite (Henze et al., 2008; Tsigaridis et al., 2014). The same models  
125 indicate that the formation of SOA from biogenic sources greatly exceeds that from  
126 anthropogenic sources. The shortcomings in many OA models are partially due to the  
127 assumption that POA is non-volatile and nonreactive (Kanakidou et al., 2005; Jimenez  
128 et al., 2009). To address these shortcomings, Donahue et al. (2006) developed the  
129 volatility basis set (VBS) framework which assumes that POA emissions are  
130 semivolatile and photochemically reactive and uses logarithmically spaced volatility  
131 bins to distribute POA upon emission. Recently, several regional-scale modeling  
132 studies have accounted for the semivolatile nature and chemical aging of organic  
133 compounds demonstrating improvements in reproducing the OA concentrations and  
134 chemical composition (Robinson et al., 2007; Shrivastava et al., 2008; Murphy and  
135 Pandis, 2009; Tsimpidi et al., 2010; Tsimpidi et al., 2011; Hodzic et al., 2010;  
136 Fountoukis et al., 2011; Bergstrom et al., 2012; Athanasopoulou et al., 2013; Zhang et  
137 al., 2013; Fountoukis et al., 2014). However, only few global modeling studies have  
138 yet adopted the VBS approach to simulate the SOA formation from the chemical  
139 aging of SVOC and IVOC emissions (Jathar et al., 2011; Tsimpidi et al., 2014;  
140 Shrivastava et al., 2015; Hodzic et al., 2015). According to these studies, the modeled  
141 tropospheric burden of POA is 0.09-0.94 Tg and of SOA 1.8-2.8 Tg.

142 In this work we use ORACLE, a computationally efficient module for the  
143 description of organic aerosol composition and evolution in the atmosphere (Tsimpidi

144 et al., 2014), to estimate the impact of open biomass burning and anthropogenic  
145 combustion emissions and their chemical aging on global OA budgets and  
146 distributions. An extensive global dataset of AMS measurements and factor-analysis  
147 results from 84 field campaigns in the Northern Hemisphere are used in combination  
148 with the model results during the period of 2001-2010. This integrated effort provides  
149 further insights into the temporal and geographical variability of the OA particles,  
150 emission strengths and the chemical processing of organics from combustion sources.

151

## 152 **2. Model description and application**

153

### 154 **2.1 EMAC Model**

155 The ECHAM/MESSy Atmospheric Chemistry (EMAC) model is a numerical  
156 chemistry and climate simulation system that includes sub-models describing the  
157 lower and middle atmosphere processes (Jöckel et al., 2006). EMAC includes  
158 submodels that describe gas-phase chemistry (MECCA; Sander et al., 2011),  
159 inorganic aerosol microphysics (GMXe; Pringle et al., 2010), cloud microphysics  
160 (CLOUD; Jöckel et al., 2006), aerosol optical properties (AEROPT; Lauer et al.,  
161 2007), dry deposition (DRYDEP; Kerkweg et al., 2006a), sedimentation (SEDI;  
162 Kerkweg et al., 2006a), cloud scavenging (SCAV; Tost et al., 2006), emissions  
163 (ONLEM and OFFLEM; Kerkweg et al., 2006b), and organic aerosol formation and  
164 growth (ORACLE; Tsimpidi et al., 2014).

165 The removal of gas and aerosol organic compounds through dry deposition is  
166 calculated with the DRYDEP submodel (Kerkweg et al., 2006a) based on the big-leaf  
167 approach, and the dry deposition velocities depend on physical and chemical  
168 properties of the surface cover (e.g., the roughness length, soil pH, leaf stomatal  
169 exchange, etc.). The sedimentation of aerosols is calculated with the SEDI submodel  
170 (Kerkweg et al., 2006a) using a first-order trapezoid scheme. In-cloud scavenging and  
171 rainout of gas and aerosol species are treated by the SCAV submodel (Tost et al.,  
172 2006). The effective Henry's law coefficient used for calculating the scavenging rates  
173 of LVOCs, SVOCs, and IVOCs is  $10^5 \text{ M atm}^{-1}$ .

174 The spectral resolution used in this study is T63L31, corresponding to a horizontal  
175 grid resolution of  $1.875^\circ \times 1.875^\circ$  and 31 vertical layers extending to 10 hPa at about 25  
176 km altitude. EMAC has been run for 11 years, covering the period 2000–2010, and

177 the first year is used as spin-up. EMAC has been extensively described and evaluated  
178 against in situ observations and satellite measurements that include filter-based  
179 particulate matter concentrations, aerosol optical depth, acid deposition, gas-phase  
180 mixing ratios, and meteorological parameters (Jöckel et al., 2006; Pozzer et al.,  
181 2012a; Pozzer et al., 2012b; Karydis et al., 2016). Tsimpidi et al. (2014) performed an  
182 in depth evaluation of the EMAC calculated total OA over different continents by  
183 using measurements from the EMEP network over Europe, the IMPROVE network  
184 over North America, and several short-term field campaigns over East Asia,  
185 subtropical West Africa, the Amazon rainforest, and the Canadian boreal forest. The  
186 present work focuses on the model evaluation for the individual OA components (i.e.,  
187 POA and SOA). In addition, the statistical evaluation of EMAC results for the  
188 inorganic components summarized in Tables S1-S3 in the Supplementary Material.

189

## 190 **2.2 ORACLE Module**

191 ORACLE is a computationally efficient submodel for the description of OA  
192 composition and evolution in the atmosphere which has been implemented into the  
193 EMAC model by Tsimpidi et al. (2014). ORACLE simulates a variety of semivolatile  
194 organic species and reaction products and separates them into groups of compounds  
195 with logarithmically spaced effective saturation concentrations.

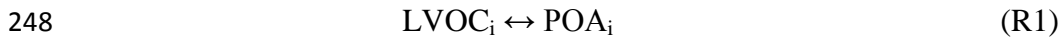
196 In this study, primary organic emissions from open biomass burning and from  
197 anthropogenic sources (i.e., fossil fuel and biofuel) are simulated using separate  
198 surrogate species for each source category. They are subdivided into three groups of  
199 organic compounds: low volatility, LVOCs ( $10^{-2} \mu\text{g m}^{-3}$ ), semi-volatile, SVOCs ( $10^0$   
200 and  $10^2 \mu\text{g m}^{-3}$ ) and intermediate volatility organic compounds, IVOCs ( $10^4$  and  $10^6 \mu\text{g}$   
201  $\text{m}^{-3}$ ). These organic compounds are allowed to partition between the gas and aerosol  
202 phases resulting in the formation of fPOA (anthropogenic POA from fossil fuel and  
203 biofuel combustion) and bbPOA (natural POA from open biomass burning). VOCs are  
204 distinguished into anthropogenic and biogenic and their oxidation products are  
205 distributed in four volatility bins with effective saturation concentrations of  $10^0$ ,  $10^1$ ,  
206  $10^2$ , and  $10^3 \mu\text{g m}^{-3}$  at 298 K by using the aerosol mass yields (Table S4) by Tsimpidi  
207 et al., (2014). Gas-phase photochemical reactions that change the volatility of the  
208 organics are taken into account and their oxidation products (SOA-sv, SOA-iv, and  
209 SOA-v) are simulated separately in the module to keep track of their origin. The

210 suffixes –sv, -iv and -v to the term SOA define category of precursors (SVOCs,  
211 IVOCs, and VOCs, respectively). For the current application, SOA components are  
212 divided into four groups based on their source: anthropogenic from fossil fuel and  
213 biofuel combustion sources (fSOA), natural from open biomass burning (bbSOA),  
214 SOA from anthropogenic (aSOA-v) and biogenic (bSOA-v) VOCs. This study focuses  
215 on the OA produced from primary combustion sources and discusses in detail results  
216 for the first two types of SOA (fSOA and bbSOA). The model set up for simulating the  
217 formation of aSOA-v and bSOA-v and the corresponding results can be found in  
218 Tsimpidi et al. (2014). In addition, in this work ORACLE has been modified to  
219 distinguish the formation of fresh SOA and aged SOA by adding additional tracers to  
220 the model. The first generation oxidation products of SVOCs, IVOCs, and VOCs are  
221 characterized as fresh while SOA produced from any additional oxidation step is  
222 grouped together and considered aged (Figure 1). LVOCs are not allowed to  
223 participate in photochemical reactions since they are in the lowest volatility bin. This  
224 assumption may introduce a small bias in our results only under extremely clean  
225 conditions ( $OA \leq 10^{-2} \mu\text{g m}^{-3}$ ) where part of LVOC is in the gas phase. Adding another  
226 bin in the volatility distribution to accurately represent the extremely low volatility  
227 organic compounds (e.g., ELVOCs with  $C^*$  lower than  $10^{-3}$ ) would be useful only for  
228 studying new particle formation, which is outside the scope of the current work. The  
229 volatilities of SVOCs and IVOCs are reduced by a factor of  $10^2$  as a result of the OH  
230 reaction with a rate constant of  $2 \times 10^{-11} \text{ cm}^3 \text{ molecule}^{-1} \text{ s}^{-1}$  and a 15% increase in mass  
231 is assumed to account for two added oxygen atoms (Tsimpidi et al., 2014). This  
232 formulation is comparable to a number of global and regional studies which assume  
233 two orders of magnitude reduction in volatility and up to 50% increase in mass per  
234 reaction (Grieshop et al. 2009; Hodzic et al., 2010; Pye and Seinfeld 2010, etc.).  
235 Shrivastava et al. (2011) even used seven orders of magnitude reduction in volatility  
236 per reaction. However, despite the fact that most of the studies assume that each  
237 oxidation reaction of SVOC and IVOC reduces the volatility of the precursor by one  
238 (e.g., Tsimpidi et al., 2010; Jathar et al., 2011; Bergstrom et al., 2012) or two orders of  
239 magnitude, the oxidation products can be up to four orders of magnitude lower in  
240 volatility than the precursor (Kroll and Seinfeld, 2008). Furthermore, ORACLE  
241 calculates the fraction of the semivolatile organic compounds that condenses to (or  
242 evaporates from) the particle phase by assuming bulk equilibrium and that all organic

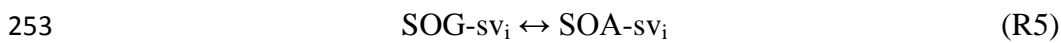
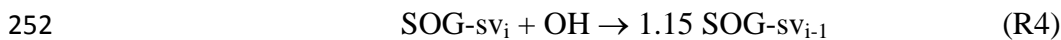
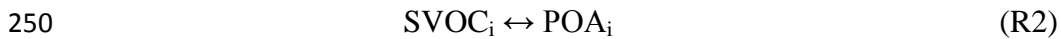


243 compounds form a pseudo-ideal solution (Tsimpidi et al., 2014). Overall, the primary  
244 aerosol formation from the phase partitioning of the freshly emitted LVOCs and  
245 SVOCs, as well as the formation of SOA from the photo-oxidation of SVOCs and  
246 IVOCs are described by the following reactions:

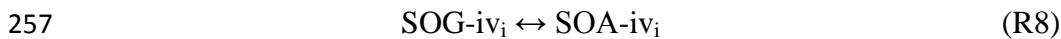
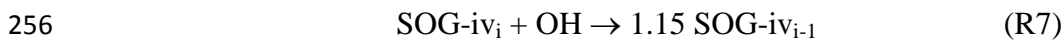
247



249



254



258

259 where  $i$  is the original volatility bin and  $i-1$  is the volatility bin with saturation  
260 concentration reduced by a factor of  $10^2$ . The term SOG corresponds to secondary  
261 organic gas that is produced by at least one chemical reaction in the atmosphere. The  
262 symbol “ $\leftrightarrow$ ” denotes the equilibrium between the gas and the aerosol phases. It is  
263 worth mentioning that the production of  $\text{RO}_2$  as an intermediate after the oxidation of  
264 SVOC and IVOC has been omitted since it would be essential only in cases where  
265 these reactions are a potentially significant sink of OH (i.e. in concentrated smoke  
266 plumes) (Alvarado et al., 2015). The model set-up and the different aerosol types and  
267 chemical processes that are simulated by ORACLE for this study are illustrated in  
268 Figure 1. More details about ORACLE can be found in Tsimpidi et al. (2014).

269

### 270 **2.3 Emission inventory**

271 The CMIP5 RCP4.5 emission inventory (Clarke et al., 2007) is used for the  
272 anthropogenic POA emissions from fossil fuel and biofuel combustion sources. The  
273 open biomass burning emissions from savanna burning and forest fires are based on  
274 the Global Fire Emissions Database (GFED v3.1; van der Werf et al., 2010). These  
275 emission datasets report the mass of the OC emitted. Therefore, in order to determine

276 the total organic matter (OM) emitted (including any additional species associated  
277 with the carbon) OM/OC values of 1.3 for anthropogenic POA and 1.6 for open  
278 biomass burning POA are used. These values are based on the OM:OC ratios  
279 estimated by Canagaratna et al. (2015) for HOA and BBOA, respectively.  
280 Furthermore, the above emission datasets are monthly resolved and treat POA as non-  
281 reactive and non-volatile. However, only a fraction of this organic material is directly  
282 emitted in the aerosol phase as POA. Most of it is rapidly transferred to the gas phase  
283 where it can undergo chemical transformations and form SOA. Therefore, key input  
284 for the accurate description of these compounds and their chemical aging is the  
285 volatility distribution at 298 K. Figure 2 depicts the volatility distributions assumed  
286 for this study which cover a range of  $10^{-2}$  to  $10^4$   $\mu\text{g m}^{-3}$  for open biomass burning  
287 (May et al., 2013) and  $10^{-2}$  to  $10^6$   $\mu\text{g m}^{-3}$  for fossil and biofuel combustion emissions  
288 (Robinson et al., 2007). Emission inventories are based on samples collected at  
289 aerosol concentrations up to  $10^4$   $\mu\text{g m}^{-3}$  (Shrivastava et al., 2008; Robinson et al.,  
290 2010). As a result IVOC emissions with  $C^* > 10^4$   $\mu\text{g m}^{-3}$  are missing from the  
291 traditional emission inventories and have to be accounted for by assigning additional  
292 emissions in this volatility range. We assume that the missing IVOC emissions from  
293 anthropogenic combustion are 1.5 times the traditional OA emissions included in the  
294 inventory (Shrivastava et al., 2008; Tsimpidi et al., 2010), therefore the sum of the  
295 emission factors is 2.5. No additional IVOC emissions are assumed in the  $C^* > 10^4$   $\mu\text{g}$   
296  $\text{m}^{-3}$  bins for open biomass burning and therefore the sum for the biomass burning  
297 emission factors is unity. As a result, 40% of the biomass burning OA emissions  
298 represents IVOCs with  $C^* = 10^4$   $\mu\text{g m}^{-3}$  (Table 2). The sensitivity of our results to  
299 these assumptions will be discussed in a subsequent article in preparation. Overall, the  
300 decadal average global emission flux of SVOCs and IVOCs is  $44 \text{ Tg yr}^{-1}$  from  
301 anthropogenic combustion sources and  $28 \text{ Tg yr}^{-1}$  from open biomass burning sources.

302

### 303 **3. Model evaluation methodology**

304

#### 305 **3.1 Factor analysis of AMS measurements**

306

307 During the period 2001-2010, 84 field campaigns were performed in the Northern  
308 Hemisphere using the AMS for measuring ambient OA concentrations in urban,

309 urban-downwind, and rural environments (Figure 3). Information for each of these  
310 campaigns is given in Tables S5-S7. The OA source apportionment for all sites was  
311 taken from the literature (Tables S5-S7) and performed using factor-analysis  
312 techniques classifying OA as HOA, corresponding to POA from fossil fuel  
313 combustion, and OOA, corresponding to SOA. Therefore, AMS HOA is compared  
314 with modeled fPOA, which is emitted and remains in the aerosol phase without  
315 undergoing chemical reactions, and AMS-OOA is compared with modeled SOA (the  
316 sum of SOA-sv, SOA-iv, and SOA-v), formed from the oxidation of gas phase  
317 precursors (SVOCs, IVOCs, and VOCs). At many locations, PMF and other factor  
318 analysis techniques identified two subtypes of OOA that differ in volatility and  
319 oxidation state: semi-volatile OOA (SV-OOA) and low-volatility OOA (LV-OOA).  
320 There are different potential interpretations of SV-OOA and LV-OOA. SV-OOA  
321 often correlates with semi-volatile species such as ammonium nitrate and is less  
322 oxygenated, consistent with relatively fresh SOA (Zhang et al., 2011; Ng et al., 2011).  
323 LV-OOA usually correlates with nonvolatile secondary species such as sulfate, and is  
324 highly oxygenated, consistent with regional aged OA (Zhang et al., 2011; Ng et al.,  
325 2011). Recently, Ehn et al. (2014) found a direct pathway which leads to the  
326 formation of fresh LV-OOA from the oxidation of several biogenic VOCs. Here we  
327 test the hypothesis that SV-OOA corresponds to the first generation products and LV-  
328 OOA to the later generation ones. Therefore, AMS SV-OOA is compared with the  
329 fraction of SOA-sv, SOA-iv, and SOA-v from the first oxidation step of SVOCs,  
330 IVOC, and VOCs as it is tracked separately (henceforth EMAC fresh SOA). Then  
331 AMS LV-OOA is compared with the fraction of SOA-sv, SOA-iv, and SOA-v from  
332 any additional oxidation step (henceforth EMAC aged SOA). Finally, in a few field  
333 campaigns, e.g., in the Alps (Lanz et al., 2010), residential wood burning was found  
334 to be a major source of OA. However, residential wood burning is included in EMAC  
335 as fPOA. To account for this inconsistency for the AMS data sets that include BBOA  
336 we compare the sum of the simulated fPOA and bbPOA (henceforth EMAC POA) to  
337 the sum of the AMS HOA and BBOA (henceforth AMS POA). In data sets where OA  
338 from cooking activities has been resolved by the PMF analysis, AMS COA has not  
339 been taken into account for the model evaluation since these emissions are not  
340 included in our emission inventory.

341

### 342 3.2 Evaluation metrics

343

344 The mean bias (MB), mean absolute gross error (MAGE), normalized mean bias  
345 (NMB), normalized mean error (NME), and the root mean square error (RMSE) are  
346 used to assess the model performance:

$$347 \quad MAGE = \frac{1}{N} \sum_{i=1}^N |P_i - O_i| \quad (1) \quad MB = \frac{1}{N} \sum_{i=1}^N (P_i - O_i) \quad (2)$$

$$348 \quad NME = \frac{\sum_{i=1}^N |P_i - O_i|}{\sum_{i=1}^N O_i} \quad (3) \quad NMB = \frac{\sum_{i=1}^N (P_i - O_i)}{\sum_{i=1}^N O_i} \quad (4)$$

$$349 \quad RMSE = \left[ \frac{1}{N} \sum_{i=1}^N (P_i - O_i)^2 \right]^{\frac{1}{2}} \quad (5)$$

350 where  $O_i$  is the observed campaign average value of the  $i$ th OA component,  $P_i$  is the  
351 corresponding modelled value during the same period, and  $N$  is the total number of  
352 comparisons used for the evaluation. NME (in %) and MAGE (in  $\mu\text{g m}^{-3}$ ) provide an  
353 estimate of the overall discrepancy between predictions and observations, while NMB  
354 (in %) and MB (in  $\mu\text{g m}^{-3}$ ) are sensitive to systematic errors. RMSE (in  $\mu\text{g m}^{-3}$ ) is the  
355 root of the mean square error, which incorporates both the variance of the prediction  
356 and its bias. Both NME and MAGE inherently include the corresponding bias, which  
357 is the reason why their magnitude is equal or larger than NMB and MB respectively.  
358 For an unbiased prediction, NME and MAGE express the variance. When NME and  
359 NMB or MAGE and MB are close, the discrepancy is explained as a systematic bias  
360 rather than scatter. When NME/MAGE exceeds NMB/MB, part of the discrepancy  
361 between predictions and observations is explained as scatter. To determine the effects  
362 of the site type, geographical location and the seasonal cycle on the model results, the  
363 evaluation metrics are calculated separately for urban, urban-downwind, and rural  
364 sites; European, North American, and Asian sites; and for four seasons (winter,  
365 spring, summer, and autumn).

366

### 367 4. Model results

368

## 369 4.1 OA from anthropogenic combustion

370

### 371 4.1.1 Geographical distribution

372 Figure 4 depicts the simulated, decadal average global surface concentrations of  
373 fPOA and fSOA from anthropogenic SVOC and IVOC sources (fossil and biofuel  
374 combustion). The average surface concentration of fPOA is  $0.1 \mu\text{g m}^{-3}$ . Higher fPOA  
375 concentrations (up to  $14 \mu\text{g m}^{-3}$ ) are simulated over densely populated and highly  
376 industrialized areas (e.g., Eastern China, Northern India, Central Europe, etc.) where  
377 there are substantial anthropogenic combustion emissions. Downwind of the sources  
378 fPOA concentrations decrease substantially since they are diluted and a large fraction  
379 is predicted to evaporate during transport. This results in a highly inhomogeneous  
380 spatial distribution of fPOA concentrations (Figure 4a). In contrast, fSOA is more  
381 regionally distributed with high concentrations (up to  $9.5 \mu\text{g m}^{-3}$ ) downwind of the  
382 anthropogenic sources due to its continuous production and long-range transport from  
383 SVOCs and IVOCs (Figure 4b). This results in a continental fSOA background of  
384  $0.5\text{-}1 \mu\text{g m}^{-3}$  and in concentrations of around  $1 \mu\text{g m}^{-3}$  over marine regions close to  
385 anthropogenic sources (e.g., Arabian Sea, Yellow Sea). The average surface  
386 concentration of fSOA is  $0.26 \mu\text{g m}^{-3}$  with 73% of it originating from the oxidation of  
387 IVOC emissions. This result supports the hypothesis of several recent studies that  
388 IVOC emission and oxidation may be a significant SOA source that has been missing  
389 from chemistry climate models (Jathar et al., 2011; Tsimpidi et al., 2014). The  
390 relatively small contribution (25%) of SVOCs to total fSOA follows from its low  
391 emissions compared to the IVOCs (two times lower) and by the fact that a significant  
392 fraction of SVOCs stays in the aerosol phase (as POA) without undergoing chemical  
393 reactions (Tsimpidi et al., 2014).

394 The fraction of fossil and biofuel combustion OA (fOA) that is formed through the  
395 oxidation of gas phase species, fSOA/fOA, is consistently high with values ranging  
396 from around 20% close to the sources to 100% away in remote regions with a global  
397 average of 83% at the surface (Figure 5a). This suggests that over urban areas both  
398 fPOA and fSOA contribute significantly to the overall OA mass while further  
399 downwind and in rural areas SOA formation dominates since POA decreases  
400 substantially due to dilution and evaporation. The OA due to anthropogenic  
401 combustion sources contributes significantly to total OA over the continents in the

402 Northern Hemisphere (Figure 5b). The highest contribution is predicted over Eastern  
403 China (83%) and the lowest over the Southeastern US (23%). Over mid-latitude  
404 oceans, the contribution of fOA to total OA is also high (around 60%) due to the long-  
405 range transport of SOA. On the other hand, fOA/OA is very low (0-10%) over the  
406 tropical and boreal forest regions in contrast to the significant bbOA and bSOA-v  
407 concentrations over these areas. The eastern part of the Eurasian boreal forest is an  
408 exception since the lower emissions of bbOA together with the considerable amount  
409 of fSOA transported from Europe results in fOA/OA fractions of about 40%. Overall,  
410 the predicted global average fOA/OA is 38%. This result highlights the importance of  
411 anthropogenic emissions for global OA levels, also suggested by other recent studies  
412 (Carslaw et al., 2013; Lee et al., 2013; Spracklen et al., 2011).

413

#### 414 **4.1.2 Temporal profile**

415 Table 1 shows the decadal average tropospheric burden of fPOA and fSOA. The  
416 decadal average tropospheric burden of total fOA is 0.63 Tg (10% fPOA and 90%  
417 fSOA). The tropospheric fSOA/fOA is higher than at the surface since SVOC and  
418 IVOC continue forming fSOA at higher altitudes (Tsimpidi et al., 2014).

419 The wintertime burden of fPOA is 36% higher than its annual average value  
420 (Figure 6a). This increase is partially driven by the seasonality of the emissions since  
421 anthropogenic OA emissions are 12% higher during winter compared to the annual  
422 average. Furthermore, the lower temperatures that occur during winter in the Northern  
423 Hemisphere drive the gas-particle partitioning of freshly emitted SVOCs to the  
424 aerosol phase resulting in higher fPOA concentrations. At the same time, less SVOCs  
425 are available in the gas phase to react with the lower wintertime OH resulting in  
426 reduced formation of fSOA. The wintertime tropospheric burden of fSOA is 16%  
427 lower than the annual average value (Figure 6a) representing 87% of the fOA. During  
428 summer, the photooxidation of SVOC and IVOC is significantly enhanced; however,  
429 the increase in fSOA mass is compensated by evaporation due to the high  
430 temperatures resulting in an overall increase of only 3% compared to the annual  
431 average values. High temperatures during summer also result in a significant decrease  
432 of fPOA due to evaporation, i.e., a 27% decrease compared to the annual average  
433 tropospheric burden (Figure 6a). Overall, the tropospheric fSOA:fOA during summer  
434 increases to 93%. The highest fSOA concentrations are predicted during spring (i.e.,

435 April) when photochemistry is active and the moderately low temperatures favor the  
436 partitioning into the aerosol phase (Figure 6a).

437 Figure 6b depicts the annual tropospheric fOA variability over the simulated years  
438 (2001 to 2010). The variability of the model predicted fOA is very low ( $\pm 4\%$ ) since  
439 anthropogenic emissions are assumed to have small differences between the simulated  
440 years (Clarke et al., 2007). The anthropogenic OC emissions from fossil and biofuel  
441 combustion increase by  $1.23 \text{ Tg C yr}^{-1}$  (10%) during the simulated decade. Over Asia  
442 and Africa, anthropogenic OC emissions have increased by 12% and 33%,  
443 respectively, during the simulated decade. On the other hand, anthropogenic OC  
444 emissions over North America have decreased by 15% during the same period. Over  
445 South America, anthropogenic OC emissions have decreased up to the year 2005  
446 (10%) and then remained about constant until the end of the decade. Over Europe,  
447 anthropogenic OC emissions have increased up to the year 2005 (5%) and then started  
448 to decrease reaching 4% lower emissions (compared to 2001) by the end of the  
449 decade. However, the simulated fOA tropospheric burdens over the continents (Figure  
450 6b) do not reflect this clear trend of emissions since other factors (i.e., meteorology)  
451 play an important role. Overall, the lowest fOA global tropospheric burden is  
452 calculated during the years 2001 and 2003 ( $0.61 \text{ Tg yr}^{-1}$ ) and the highest during the  
453 year 2009 ( $0.66 \text{ Tg yr}^{-1}$ ).

454

## 455 **4.2 OA from open biomass burning**

456

### 457 **4.2.1 Geographical distribution**

458 Figure 7 depicts the simulated decadal average global surface concentrations of  
459 bbPOA and bbSOA. The average surface concentration of bbPOA is  $0.11 \mu\text{g m}^{-3}$ . The  
460 highest bbPOA concentrations (up to  $7.7 \mu\text{g m}^{-3}$ ) are predicted over the tropical  
461 rainforests (i.e., Amazon, Congo, and Southeast Asia) and the boreal forests (i.e.,  
462 Alaska, Canada, and Russia) due to substantial emissions from forest and savannah  
463 fires. Similar to fPOA, bbPOA levels rapidly decrease as the air masses travel from  
464 the sources due to dilution and evaporation (Figure 7a). The average surface  
465 concentration of bbSOA is  $0.15 \mu\text{g m}^{-3}$ . In contrast to anthropogenic combustion  
466 emissions, IVOCs are assumed to account for only 40% of the total open biomass  
467 burning emissions. Nevertheless, the model predicts that the bbSOA formed due to

468 the oxidation of IVOCs (46%) is similar to that from the oxidation of SVOCs (54%).  
469 This result corroborates our finding that IVOCs are a significant source of SOA.  
470 bbSOA concentrations are more spatially homogeneous compared to bbPOA reaching  
471 high levels (up to  $6.4 \mu\text{g m}^{-3}$ ) over a wide area covering most of South America,  
472 Central and South Africa, Southeastern Asia, including Indonesia (Figure 7b). The  
473 atmosphere over the South Atlantic Ocean is also strongly influenced by long-range  
474 transport of bbSOA from the Congo Basin ( $1\text{-}3 \mu\text{g m}^{-3}$ ). Over these areas, the  
475 atmospheric conditions are favorable for the photochemical oxidation of SVOCs and  
476 IVOCs. On the other hand, over the boreal forests, the low temperatures favor the  
477 partitioning of SVOCs into the particulate phase forming bbPOA, and at the same  
478 time the photo-oxidation of IVOCs is slow. This results in moderate average bbSOA  
479 concentrations around  $0.5 \mu\text{g m}^{-3}$ .

480 Figure 8a depicts the predicted decadal average contribution of bbSOA to total  
481 bbOA (bbSOA/bbOA) at the surface. bbSOA/bbOA is high with values ranging from  
482 around 35% over the tropical and boreal forests to 85% in areas downwind and over  
483 the oceans. The global average bbSOA/bbOA at the surface is predicted to be 72%.  
484 This result indicates that even though the biomass burning emissions are distributed in  
485 relatively low volatility bins ( $C^* \leq 10^4 \mu\text{g m}^{-3}$ ), bbSOA still exceeds primary biomass  
486 burning OA on a global scale. Figure 8b depicts the decadal average surface  
487 contribution of bbOA to total OA (bbOA/OA). As expected, bbOA contributes  
488 significantly to total OA over the tropical and boreal forests (around 60%) while it has  
489 a smaller impact on OA levels over the mid-latitude continents of the Northern  
490 Hemisphere. This result does not include other types of biomass combustion (e.g., for  
491 residential heating) that often contribute significantly in urban areas (Chen et al.,  
492 2007; Wang et al., 2007; Lanz et al., 2010). High bbOA contributions are also  
493 predicted downwind of the boreal forests (up to 80%). Furthermore, the bbOA/OA  
494 ratio is high (50-90%) off the west coasts of Africa, South America and Indonesia.  
495 These high values are due to the chemical aging of biomass burning SVOCs and  
496 IVOCs in contrast to the chemical products of biogenic VOCs which are not allowed  
497 to participate in additional photochemical reactions (Tsimpidi et al., 2014). Overall,  
498 the global average bbOA/OA is predicted to be 26%.

499

#### 500 **4.2.2 Temporal evolution**



501 The decadal average tropospheric burden of total bbOA is  $0.59 \text{ Tg yr}^{-1}$  (30%  
502 bbPOA, 70% bbSOA) (Table 1). The fraction of bbOA that is secondary is less than  
503 that of fOA (90%).

504 The interannual variability of bbPOA and bbSOA is high due to the seasonality of  
505 fires (Figure 9a). During July to September (dry season) intense wildfires are reported  
506 over the tropics related to the low precipitation and high temperatures. This results in  
507 high biomass burning emissions which together with the intense photochemical  
508 activity result in bbOA tropospheric burdens of up to  $1.4 \text{ Tg yr}^{-1}$  during August  
509 (130% higher than the annual average). The lowest bbOA tropospheric burdens are  
510 estimated during the wet season ( $0.21 \text{ Tg yr}^{-1}$  during April, 64% lower than the annual  
511 average). Furthermore, during the dry season OA consists mainly of bbOA over the  
512 tropical rainforests due to the intense wildfires while during the wet season OA  
513 consists mainly of biogenic SOA since biomass burning emissions are low. As a  
514 result, the bbOA/OA has a significant seasonal variability as well; during the dry  
515 season the global average bbOA/OA increases significantly (e.g., 41% during August;  
516 not shown) while during the wet season it is significantly lower (e.g., 11% during  
517 March; not shown).

518 The decadal variability of the model predictions is also important since open  
519 biomass burning emissions can vary significantly from year to year (Figure 9b). The  
520 years 2001 and 2009 had relatively low fire activity ( $13.5 \text{ Tg C yr}^{-1}$ ) and the bbOA  
521 annual tropospheric burden was  $0.47 \text{ Tg yr}^{-1}$  (21% lower than the decadal average).  
522 During these two years tropospheric bbOA was lower over both the Amazon and the  
523 Congo basin (Figure 9b). The year of 2010 on the other hand was characterized by  
524 severe wildfires, especially in the Amazon region (OC emissions were twice the  
525 decadal average) resulting in a global bbOA source of  $0.72 \text{ Tg yr}^{-1}$  (21% higher than  
526 the decadal average). Over the Congo Basin, the calculated tropospheric burden peaks  
527 during the years 2005 and 2010 (Figure 9b) while over the Amazon Basin, the highest  
528 burdens are calculated during the years 2007 and 2010. The above results are  
529 consistent with Chen et al. (2013) who analyzed satellite data to detect the fire activity  
530 over the Amazon rainforest and reported a twofold increase in fire activity during  
531 2010 compared to 2009.

532

533 **5. Comparison with AMS data**

534

## 535 **5.1 Evaluation over urban areas**

536 The spatial resolution used in the current application as well as in most global  
537 model applications (Tsigaridis et al., 2014) can introduce potentially significant errors  
538 over urban areas. Other issues can also add to the model/measurement discrepancy  
539 over cities. For example, global models, including EMAC, lack OA emissions from  
540 residential and commercial cooking activities (Tsigaridis et al., 2014). However,  
541 cooking can be an important source of OA that can contribute significantly to  
542 measured POA (around 50%) and total OA (15%-20%) over urban areas (Sun et al.,  
543 2011; Mohr et al., 2012; Ge et al., 2012; Hayes et al., 2013). Therefore our analysis  
544 and use of the corresponding urban AMS datasets should be viewed as an effort to  
545 quantify the magnitude of these errors. In addition, there have been a number of  
546 recent studies using global atmospheric chemistry models to investigate the link  
547 between premature mortality and atmospheric aerosols in urban and rural  
548 environments (Lelieveld et al., 2015). Evaluating global models over urban locations  
549 can provide useful information about their potential biases in these locations.

550 AMS observations indicate that over urban areas the POA (sum of HOA and  
551 BBOA) concentration is relatively high while further downwind and in rural areas it  
552 decreases substantially due to dilution and evaporation (Figure 10a). The model is  
553 able to reproduce this trend, however, it significantly underpredicts (NMB=-65%,  
554 Table 2) the high values of POA over urban areas and especially over densely  
555 populated areas such as Beijing, Tokyo and Mexico City (Table S5; Figure 11a). This  
556 underprediction appears to be typical for global models (Tsigaridis et al., 2014) and is  
557 partly associated with the limited spatial resolution of the model (the size of a grid  
558 cell used typically exceeds the size of most urban centers) and the lack of COA  
559 emissions. The model underestimates SOA (NMB=-33%, Table 2) over densely  
560 populated areas such as Beijing and Mexico City (Table S5; Figure 12a) partially due  
561 to its limited spatial resolution. In addition, the lack of COA emissions can be  
562 considered as a possible cause of OOA underestimation by the model over urban and  
563 urban-downwind areas (see below) given that COA can be oxidized and form SOA  
564 over the urban center and further downwind. Overall, the underestimation of OA over  
565 urban locations indicates that global exposure studies (Lelieveld et al., 2015) provide

566 a lower limit of the actual contribution of OA to premature mortality over large urban  
567 areas.

568 Given that the model cannot reproduce the concentrations of POA and SOA over  
569 urban locations well due to the coarse spatial resolution and lack of COA emissions,  
570 urban locations are not included for the seasonal, continental and total (annual)  
571 evaluation of the model presented below. Especially for the seasonal model  
572 evaluation, most of the urban field campaigns were conducted either during winter or  
573 summer. Therefore, including these locations in our analysis is expected to bias the  
574 model performance during winter and summer leading to a potential misinterpretation  
575 of the corresponding seasonal results.

576

## 577 **5.2 Spatial evaluation**

578

### 579 **5.2.1 POA**

580 Over urban-downwind locations, the model does a better job than urban locations  
581 in reproducing the measured POA values (Table 3). This can be verified by focusing  
582 on specific field campaigns that provide data from both the urban center and urban-  
583 downwind locations over the same period of time (i.e., MILAGRO over Mexico City  
584 and MEGAPOLI over Paris). Over these areas the model captures the measured POA  
585 concentrations downwind of the urban center (Table S6; Figure 11b) but it  
586 significantly underpredicts the POA concentrations measured in the urban center  
587 (Table S5; Figure 11a). Overall, in urban-downwind and rural areas the model  
588 captures the lower POA levels (Figure 10a; Figure 11). Over urban-downwind areas,  
589 the model slightly underpredicts POA (NMB=-15%) while over rural areas it  
590 overpredicts by  $0.04 \mu\text{g m}^{-3}$  (Table 3). However, over rural areas with high BBOA  
591 concentrations (e.g, Massognex, Payerne, etc.) the model underpredicts POA (Table  
592 S7; Figure 11c) indicating that biomass burning and/or biofuel use in residential areas  
593 may be underestimated in the emission inventory.

594 In Europe, the model underestimates POA concentrations (NMB=-23%; Table 3).  
595 However, the comparison of simulated fPOA with AMS HOA (i.e, excluding BBOA  
596 from the comparison) suggests that the model overpredicts POA over Europe with a  
597 NMB=20% (not shown). This result underscores the underestimated emissions from  
598 residential biofuel use as a prominent cause of the model bias over Europe. The

599 possible underestimation of biomass/biofuel burning emissions in European  
600 residential areas has also been reported by other studies (Bergstrom et al., 2012;  
601 Kostenidou et al., 2013; Denier van der Gon et al., 2015). Over North America, the  
602 model reproduces well the measured HOA (Table 3). Over Asia, the model  
603 overestimates the low values of POA measured by AMS (Table 3) mainly due to the  
604 high simulated bbPOA concentrations (45% of total POA) transported from the boreal  
605 forests of Northeast Asia.

606

### 607 **5.2.2 SOA**

608 Both AMS and EMAC model results indicate that SOA (and OOA) is high over all  
609 environments considered (Table 4). The highest concentrations are found over urban  
610 locations (AMS-OOA=  $4.33 \mu\text{g m}^{-3}$  and EMAC-SOA=  $2.97 \mu\text{g m}^{-3}$ ) while further  
611 downwind SOA concentrations decrease by 37% over rural locations according to  
612 both AMS and EMAC results (Figure 10b). This indicates that the initial emissions of  
613 VOCs, IVOCs and SVOCs are photo-oxidized rapidly in the urban environment  
614 producing SOA, while their atmospheric aging and further production of SOA is  
615 offset by dilution as the air masses travel from the urban centers. EMAC does a  
616 reasonable job in reproducing SOA concentrations (Table 4), however, a systematic  
617 underprediction is found in all types of environments. The best model performance is  
618 achieved over urban downwind locations (NMB=-25%) followed by urban and rural  
619 areas (NMB=-31% and -32%, respectively). The model significantly underpredicts  
620 SOA over specific urban-downwind and rural areas. In most of these cases the field  
621 campaign was short (up to 1 week) and the results were subject to specific pollution  
622 episodes which cannot be captured by our model (e.g., Puy de Dome, Table S7;  
623 Figure 12c).

624 Over the continents, the largest SOA underestimation is found over Europe  
625 (NMB=-39%). Similar to POA, it is mostly driven by the model underperformance  
626 over sites with high biomass burning sources and biofuel use (e.g, Harkingen and  
627 Payern, CH; Figure 12). Over North America, the model simulates well the SOA  
628 formation with NMB=-15%. IEPOX-SOA, a type of SOA likely formed via  
629 processing of later generation isoprene products in aqueous acidic aerosols, has been  
630 recently suggested as an important source of SOA close to isoprene emissions (Hu et  
631 al., 2015). The model does not simulate SOA formation from aqueous-phase reactions

632 and therefore does not produce IEPOX-SOA, which may lead to an underestimation  
633 of SOA over some sites in North America that are strongly influenced by isoprene  
634 emissions (e.g. over the Pinnacle state park, NY; Table S7; Figure 12c). Over Asia,  
635 the model slightly underestimates SOA with NMB=-22% (Table 4; Figure 12).

636 In most of the available datasets (41 out of 84), PMF provides information for the  
637 two subtypes of OOA (LV-OOA and SV-OOA). Both PMF and EMAC results  
638 indicate that aged SOA (or LV-OOA) is higher than fresh SOA (or SV-OOA)  
639 regardless of the type of environment (Tables 5, 6). However, in North America,  
640 AMS SV-OOA is slightly higher than LV-OOA while EMAC calculations indicate  
641 the opposite (Tables 5, 6). Despite this discrepancy, the model reproduce well both  
642 the fresh SOA (NMB=-29%) and aged SOA (NMB=-20%) over North America while  
643 over Europe the underestimation is larger (Tables 5, 6) The EMAC performance is  
644 better over urban locations where it reproduces the high levels of aged SOA with  
645 NMB=-21% and NME=43% (Table 2). Over urban-downwind and rural locations  
646 EMAC underpredicts aged SOA with NMB=-47% and -38%, respectively (Table 5).  
647 The performance of the model for fresh SOA is better compared to aged SOA (Table  
648 5), with the exception of North America, indicating that the modeled OA aging  
649 parameterization may underestimate the SOA produced from chemical reactions  
650 during transport and requires improvements. Similar to aged SOA, the best  
651 performance of the model for fresh SOA is obtained over urban locations (NMB=-  
652 12%).

653

### 654 **5.3 Seasonal evaluation**

655

#### 656 **5.3.1 POA**

657 The model performs best during summer (RMSE=0.4, NMB=-3%), followed by  
658 autumn (RMSE=0.37, NMB=-15%) and spring (RMSE=0.52, NMB=21%). During  
659 winter EMAC underpredicts POA with NMB=-34% (Table 3; Figure 13a). This result  
660 corroborates our hypothesis that residential biofuel emissions may be underestimated  
661 in the inventory since residential heating is expected during winter. Furthermore,  
662 since vehicle catalysts require a certain temperature to work to full efficiency,  
663 emissions from gasoline and diesel engines are significantly higher during the warm-  
664 up phase of the car (Westerholm et al., 1996). Typically, the additional emissions

665 during the warm-up phase (or cold-start emissions) are not accounted for in emission  
666 inventories, which are based on measurements at an ambient temperature of 23 °C  
667 (Weilenmann et al., 2009). However, cold-start emissions increase considerably at  
668 lower ambient temperatures varying by more than one order of magnitude between 23  
669 and -20 °C (Weilenmann et al., 2009), and thus significant underestimations of OA  
670 emissions from the transport sector can be expected during wintertime. Kopacz et al.  
671 (2010) provide a global estimate of CO sources by adjoint inversion of satellite  
672 datasets and reported an underestimation of CO sources during the winter season due  
673 to larger than expected CO emissions from vehicle cold starts and residential heating.  
674 Errors in the POA volatility distributions can also explain parts of the  
675 model/measurement discrepancy. An overestimation of the fresh POA volatility will  
676 favor its evaporation resulting in an underestimation of POA levels by the model.  
677 Another source of the POA underestimation by EMAC may be the treatment of wet  
678 deposition. The sensitivity of the results to the emission and deposition  
679 parameterizations (e.g., the Henry's law constants for the organic vapors) will be  
680 tested in a subsequent article in preparation.

681 According to recent studies (Cappa and Wilson, 2012; Aumont et al., 2012; Zhang  
682 et al., 2013), not all oxidation products of SVOCs and IVOCs can be assigned to the  
683 OOA mass fraction since they are not sufficiently oxidized. Fountoukis et al. (2014)  
684 assumed that 50% of the simulated SOA-sv and SOA-iv is still considered as HOA by  
685 the AMS analysis and found significant improvements in the view of the modeled  
686 bias for POA. In this study we tested this hypothesis and we considered POA to be the  
687 sum of fPOA and bbPOA and 50% of the SOA-sv and SOA-iv produced from the  
688 first oxidation step of SVOCs and IVOCs, respectively. We assumed that SOA-sv and  
689 SOA-iv produced during subsequent oxidation steps together with all the SOA-v are  
690 sufficiently oxidized to be considered 100% OOA. Following this hypothesis the  
691 model performance improved during winter (NME=55%  $\mu\text{g m}^{-3}$  and NMB=-28%) and  
692 autumn (NME=50%  $\mu\text{g m}^{-3}$  and NMB=1%) and deteriorated during spring  
693 (NME=110%  $\mu\text{g m}^{-3}$  and NMB=49%) and summer (NME=71%  $\mu\text{g m}^{-3}$  and  
694 NMB=16%) when the oxidation of SVOCs and IVOCs is enhanced significantly.

695

### 696 **5.3.2 SOA**

697 The best performance of the model is found for spring (NME=46%, NMB=-24%)  
698 followed by the autumn (NME=52%, NMB=-25%) and summer (NME=44%,  
699 NMB=-28%) (Table 4; Figure 13b). However, during winter the model strongly  
700 underpredicts OOA concentrations (NME=80%, NMB=-80%). The overall  
701 underprediction of OOA concentrations indicates that the model is missing an  
702 important source or formation pathway of SOA. Possible underestimation of  
703 residential biofuel emissions in our model, identified during the spatial and seasonal  
704 evaluation of simulated POA, can lead to an underestimation of SOA formed from the  
705 oxidation of these emissions during winter. Fountoukis et al. (2015) also reported low  
706 modeled SOA values compared to AMS OOA over the Paris region and attributed this  
707 discrepancy to the transformation of BBOA to OOA without the presence of sunlight  
708 reported by some recent studies (Bougiatioti et al., 2014; Crippa et al., 2013b).  
709 Underestimation of cold-start vehicle emissions during winter can also lead to a  
710 significant underestimation of SOA, since SOA produced from organic compounds  
711 emitted during the warm-up phase can be 3-7 times higher than SOA produced when  
712 the catalyst is hot (Gordon et al., 2014). Furthermore, ORACLE assumes that the only  
713 source of SOA is the homogeneous gas-phase photochemical oxidation of SOA  
714 precursors. Therefore, the negative bias of the model during winter may also be  
715 explained by its inability to simulate SOA formed from aqueous-phase and other  
716 heterogeneous reactions, including processes like oligomerization. Such processes  
717 should be taking place in all seasons. However, during the photochemically active  
718 periods (e.g., summer) there are other chemical pathways (e.g., reactions with OH and  
719 ozone) to convert the organic precursors to SOA. Adding to this the increased  
720 presence of lower-level clouds during winter and early spring compared to summer in  
721 North Hemisphere mid-latitudes (Stubenrauch et al., 2006), one would expect a higher  
722 importance of heterogeneous oxidation in winter. Finally, the underprediction of SOA  
723 by the model during winter may be also associated with an overestimation of  
724 atmospheric removal.

725 PMF and EMAC results indicate that aged SOA levels exceed those of fresh SOA  
726 during all seasons. The EMAC performance for aged SOA appears to be better during  
727 spring (NMB=-33%), summer (NMB=-36%), and autumn (NMB=-32%), and much  
728 worse during winter (NMB=-91%) (Table 5; Figure 13c). The overall performance of  
729 the model for fresh SOA (NME=60%, NMB=-30%) (Table 6, Figure 13d) appears to

730 be better than aged SOA (NME=71%, NMB=-40%) which supports our conclusions  
731 from the spatial model evaluation that the atmospheric aging of SOA may be  
732 underestimated by EMAC. However, this apparent discrepancy may be partially due  
733 to our assumption that LV-OOA corresponds only to multiple generational SOA. This  
734 is not consistent with recent studies that reported formation of LV-OOA from the first  
735 oxidation step of biogenic VOCs (Ehn et al., 2014). During winter, EMAC also  
736 underestimates the fresh SOA levels (NMB=-79%). This underprediction of both  
737 fresh and aged SOA during winter suggests that one or more important wintertime  
738 SOA formation pathways are missing in our model.

739

#### 740 **5.4 OA composition**

741 According to PMF results, the OOA/OA ratio increases downwind of the urban  
742 centers and in rural areas (from 61% over urban environments to 86% over remote  
743 areas; Figure 14a). This is generally consistent with the EMAC predictions. The  
744 predicted SOA/OA fraction increases downwind of the urban centers (from 76% over  
745 urban locations to 80% over rural areas). This change is lower than the PMF estimates  
746 but could be explained by the uncertainty of the PMF analyses (Figure 14a).  
747 Alternatively, this may indicate that EMAC tends to underpredict the aging rate of  
748 OA. OOA/OA is consistently high during all seasons (around 80%) with the highest  
749 ratio predicted in summer (90%) and the lowest in winter (74%) (Figure 14b). The  
750 model predicts high SOA/OA during all seasons except winter (Figure 14b). The  
751 highest SOA/OA ratio is predicted during summer (87%) when the photo-oxidation of  
752 SOA is enhanced. The low SOA/OA during winter (47%) once again shows the  
753 inability of EMAC model to reproduce the observed SOA levels during that season.

754 Both PMF and EMAC indicate that aged SOA is higher than fresh SOA in all types  
755 of environment and seasons (Figure 15). PMF results suggest that LV-OOA/OOA is  
756 higher over urban-downwind environments (69%), while EMAC aged SOA/SOA is  
757 similar over all types of locations (59%) (Figure 15a). The high fresh SOA fraction  
758 estimated over rural areas by both PMF and EMAC (around 40%) indicates that fresh  
759 SOA production occurs even remote from the sources. The composition of OOA  
760 exhibits a seasonal cycle as well since AMS results indicate that LV-OOA/OOA is  
761 higher during winter (73%) and lower during summer (57%) (Figure 15b). EMAC



762 predicts the highest aged SOA/SOA fraction during spring (68%) and the lowest  
763 during winter (53%) without any clear seasonal pattern (Figure 15b).

764

## 765 **6. Conclusions**

766 This study estimates the impact of open biomass burning and anthropogenic  
767 combustion emissions (from fossil and biofuels) of SVOCs and IVOCs to global OA  
768 budgets and distributions. The EMAC simulations indicate that the tropospheric  
769 burden of OA consists of 32% fOA and 30% bbOA. Furthermore, 90% of fOA and  
770 70% of bbOA is predicted to be secondary. These results support recent findings from  
771 global studies that have also reported strong contributions of SOA from  
772 anthropogenic sources to global OA concentrations (Spracklen et al., 2011; Carslaw et  
773 al., 2013; Lee et al., 2013; Tsimpidi et al., 2014).

774 The tropospheric burdens of fOA and bbOA follow a clear seasonal pattern. fOA is  
775 higher during the boreal summer (0.63 Tg) and lower during winter (0.57 Tg), while  
776 bbOA is higher during the dry season in the tropics (1.15 Tg during August) and  
777 lower during the wet season (0.17 Tg during April). The simulated spatial distribution  
778 of fOA and bbOA is driven by the sources of their precursors and atmospheric  
779 transport. Higher fPOA concentrations occur over densely populated and highly  
780 industrialized areas of the Northern Hemisphere while further downwind fPOA  
781 decreases substantially due to dilution and evaporation. On the other hand, fSOA  
782 maintains similar levels downwind of the anthropogenic sources due to the continued  
783 chemical transformations. bbPOA concentrations peak over the tropical and the boreal  
784 forests while bbSOA has high concentrations over a wide area covering most of South  
785 America, Central and South Africa, Southeastern Asia, including Indonesia and even  
786 parts of the Southern Atlantic Ocean.

787 AMS results from 84 field campaigns performed at continental locations in the  
788 Northern Hemisphere during the examined period (2001-2010) have been used to  
789 provide further insights into the composition of OA in three different types of  
790 environments: urban, urban-downwind and rural areas, during four seasons. The  
791 spatial analysis of AMS and EMAC results indicate that over urban areas POA is  
792 highest while further downwind and in rural areas decreases substantially due to  
793 dilution and evaporation. On the other hand, SOA is found to be high over all types of  
794 environments. This results in an increase of the SOA/OA ratio downwind of the urban

795 centers. The seasonal analysis of the results does not include the urban areas since the  
796 model cannot reproduce the high OA concentrations over urban environments due to  
797 its limited spatial resolution. The seasonal evaluation of the model results against the  
798 AMS measurements showed a major weakness of the model associated with  
799 calculated POA and SOA concentration levels during winter. This indicates that the  
800 model is probably missing both an important source and a formation pathway of OA,  
801 which becomes increasingly important during boreal winter. Possible causes include  
802 the underestimation of residential biofuel emissions during winter, the  
803 underestimation of vehicle cold-start emissions, the neglect of aqueous-phase and  
804 heterogeneous oxidation reactions in the model, and the overestimation of the  
805 atmospheric removal of POA and freshly formed SOA.

806 AMS results indicate that OA consists of 15% HOA and 85% OOA on average  
807 during all seasons. EMAC is able to reproduce this dominance of OOA and its results  
808 suggest that SOA accounts for 80% of total OA. At many locations, PMF analysis  
809 identified two subtypes of OOA that differ in volatility and oxidation state (LV-OOA  
810 and SV-OOA). PMF results indicate that LV-OOA is higher than SV-OOA regardless  
811 of the season or the type of environment. The overall LV-OOA/OOA fraction during  
812 the four seasons is 63% according to AMS measurement analysis. Assuming that SV-  
813 OOA corresponds to fresh SOA (first generation oxidation products) and LV-OOA  
814 corresponds to aged SOA (later generation oxidation products), EMAC is able to  
815 reproduce the PMF results predicting a dominance of aged SOA during all seasons  
816 (59% of the total SOA on average).

817

## 818 **7. Acknowledgements**

819 The research leading to these results has received funding from the European  
820 Research Council under the European Union's Seventh Framework Programme  
821 (FP7/2007-2013) / ERC grant agreement n° 226144. A.P. Tsimpidi acknowledges  
822 support from a DFG individual grand programme (project reference TS 335/2-1) and  
823 V.A. Karydis acknowledges support from a FP7 Marie Curie Career Integration Grant  
824 (project reference 618349).

825

## 826 **8. References**

827 Alvarado, M. J., Lonsdale, C. R., Yokelson, R. J., Akagi, S. K., Coe, H., Craven, J. S.,  
828 Fischer, E. V., McMeeking, G. R., Seinfeld, J. H., Soni, T., Taylor, J. W.,

829 Weise, D. R., and Wold, C. E.: Investigating the links between ozone and  
830 organic aerosol chemistry in a biomass burning plume from a prescribed fire in  
831 California chaparral, *Atmos. Chem. Phys.*, 15, 6667-6688, 10.5194/acp-15-  
832 6667-2015, 2015.

833 Aiken, A. C., Salcedo, D., Cubison, M. J., Huffman, J. A., DeCarlo, P. F., Ulbrich, I.  
834 M., Docherty, K. S., Sueper, D., Kimmel, J. R., Worsnop, D. R., Trimborn, A.,  
835 Northway, M., Stone, E. A., Schauer, J. J., Volkamer, R. M., Fortner, E., de  
836 Foy, B., Wang, J., Laskin, A., Shutthanandan, V., Zheng, J., Zhang, R.,  
837 Gaffney, J., Marley, N. A., Paredes-Miranda, G., Arnott, W. P., Molina, L. T.,  
838 Sosa, G., and Jimenez, J. L.: Mexico City aerosol analysis during MILAGRO  
839 using high resolution aerosol mass spectrometry at the urban supersite (T0) -  
840 Part 1: Fine particle composition and organic source apportionment, *Atmo.*  
841 *Chem. Phys.*, 9, 6633-6653, 2009.

842 Aiken, A. C., de Foy, B., Wiedinmyer, C., DeCarlo, P. F., Ulbrich, I. M., Wehrli, M.  
843 N., Szidat, S., Prevot, A. S. H., Noda, J., Wacker, L., Volkamer, R., Fortner, E.,  
844 Wang, J., Laskin, A., Shutthanandan, V., Zheng, J., Zhang, R., Paredes-  
845 Miranda, G., Arnott, W. P., Molina, L. T., Sosa, G., Querol, X., and Jimenez, J.  
846 L.: Mexico city aerosol analysis during MILAGRO using high resolution  
847 aerosol mass spectrometry at the urban supersite (T0) - Part 2: Analysis of the  
848 biomass burning contribution and the non-fossil carbon fraction, *Atmo. Chem.*  
849 *Phys.*, 10, 2010.

850 Athanasopoulou, E., Vogel, H., Vogel, B., Tsimpidi, A. P., Pandis, S. N., Knote, C.,  
851 and Fountoukis, C.: Modeling the meteorological and chemical effects of  
852 secondary organic aerosols during an EUCAARI campaign, *Atmos. Chem.*  
853 *Phys.*, 13, 625-645, 2013.

854 Aumont, B., Valorso, R., Mouchel-Vallon, C., Camredon, M., Lee-Taylor, J., and  
855 Madronich, S.: Modeling SOA formation from the oxidation of intermediate  
856 volatility n-alkanes, *Atmo. Chem. Phys.*, 12, 7577-7589, 2012.

857 Bahreini, R., Middlebrook, A. M., de Gouw, J. A., Warneke, C., Trainer, M., Brock,  
858 C. A., Stark, H., Brown, S. S., Dube, W. P., Gilman, J. B., Hall, K., Holloway,  
859 J. S., Kuster, W. C., Perring, A. E., Prevot, A. S. H., Schwarz, J. P., Spackman,  
860 J. R., Szidat, S., Wagner, N. L., Weber, R. J., Zotter, P., and Parrish, D. D.:  
861 Gasoline emissions dominate over diesel in formation of secondary organic  
862 aerosol mass, *Geophys. Res. Lett.*, 39, doi: 10.1029/2011gl050718, 2012.

863 Bergstrom, R., van der Gon, H. A. C. D., Prevot, A. S. H., Yttri, K. E., and Simpson,  
864 D.: Modelling of organic aerosols over Europe (2002-2007) using a volatility  
865 basis set (VBS) framework: application of different assumptions regarding the  
866 formation of secondary organic aerosol, *Atmos. Chem. Phys.*, 12, 8499-8527,  
867 2012.

868 Bougiatioti, A., Stavroulas, I., Kostenidou, E., Zampas, P., Theodosi, C., Kouvarakis,  
869 G., Canonaco, F., Prevot, A. S. H., Nenes, A., Pandis, S. N., and Mihalopoulos,  
870 N.: Processing of biomass-burning aerosol in the eastern Mediterranean during  
871 summertime, *Atmo. Chem. Phys.*, 14, 4793-4807, 2014.

872 Cappa, C. D., and Wilson, K. R.: Multi-generation gas-phase oxidation, equilibrium  
873 partitioning, and the formation and evolution of secondary organic aerosol,  
874 *Atmo. Chem. Phys.*, 12, 9505-9528, 2012.

875 Canagaratna, M. R., Jimenez, J. L., Kroll, J. H., Chen, Q., Kessler, S. H., Massoli, P.,  
876 Ruiz, L. H., Fortner, E., Williams, L. R., Wilson, K. R., Surratt, J. D., Donahue,  
877 N. M., Jayne, J. T., and Worsnop, D. R.: Elemental ratio measurements of

878 organic compounds using aerosol mass spectrometry: characterization,  
879 improved calibration, and implications, *Atmo. Chem. Phys.*, 15, 253-272, 2015  
880 Carbone, S., Aurela, M., Saarnio, K., Saarikoski, S., Timonen, H., Frey, A., Sueper,  
881 D., Ulbrich, I. M., Jimenez, J. L., Kulmala, M., Worsnop, D. R., and Hillamo,  
882 R. E.: Wintertime Aerosol Chemistry in Sub-Arctic Urban Air, *Aerosol Sci.*  
883 *Tech.*, 48, 313-323, 2014.  
884 Carslaw, K. S., Lee, L. A., Reddington, C. L., Mann, G. W., and Pringle, K. J.: The  
885 magnitude and sources of uncertainty in global aerosol, *Faraday Discuss.*, 165,  
886 495-512, 2013.  
887 Chen, L. W. A., Watson, J. G., Chow, J. C., and Magliano, K. L.: Quantifying PM<sub>2.5</sub>  
888 source contributions for the San Joaquin Valley with multivariate receptor  
889 models, *Environ. Sci. Tech.*, 41, 2818-2826, 2007.  
890 Chen, Q., Farmer, D. K., Rizzo, L. V., Pauliquevis, T., Kuwata, M., Karl, T. G.,  
891 Guenther, A., Allan, J. D., Coe, H., Andreae, M. O., Poschl, U., Jimenez, J. L.,  
892 Artaxo, P., and Martin, S. T.: Submicron particle mass concentrations and  
893 sources in the Amazonian wet season (AMAZE-08), *Atmo. Chem. Phys.*, 15,  
894 3687-3701, 2015.  
895 Chen, Y., Morton, D. C., Jin, Y., Gollatz, G. J., Kasibhatla, P. S., van der Werf, G. R.,  
896 DeFries, R. S., and Randerson, J. T.: Long-term trends and interannual  
897 variability of forest, savanna and agricultural fires in South America, *Carbon*  
898 *Management*, 4, 617-638, 2013.  
899 Chirico, R., DeCarlo, P. F., Heringa, M. F., Tritscher, T., Richter, R., Prevot, A. S. H.,  
900 Dommen, J., Weingartner, E., Wehrle, G., Gysel, M., Laborde, M., and  
901 Baltensperger, U.: Impact of aftertreatment devices on primary emissions and  
902 secondary organic aerosol formation potential from in-use diesel vehicles:  
903 results from smog chamber experiments, *Atmo. Chem. Phys.*, 10, 11545-11563,  
904 2010.  
905 Clarke, L., Edmonds, J., Jacoby, H., Pitcher, H., Reilly, J., and Richels, R.: Scenarios  
906 of greenhouse gas emissions and atmospheric concentrations (Part A) and  
907 review of integrated scenario development and application (Part B). A report by  
908 the U.S. climate change science program and the subcommittee on global  
909 change research, 2007.  
910 Crippa, M., El Haddad, I., Slowik, J. G., DeCarlo, P. F., Mohr, C., Heringa, M. F.,  
911 Chirico, R., Marchand, N., Sciare, J., Baltensperger, U., and Prevot, A. S. H.:  
912 Identification of marine and continental aerosol sources in Paris using high  
913 resolution aerosol mass spectrometry, *Journal of Geophysical Research-*  
914 *Atmospheres*, 118, 1950-1963, 10.1002/jgrd.50151, 2013a.  
915 Crippa, M., DeCarlo, P. F., Slowik, J. G., Mohr, C., Heringa, M. F., Chirico, R.,  
916 Poulain, L., Freutel, F., Sciare, J., Cozic, J., Di Marco, C. F., Elsasser, M.,  
917 Nicolas, J. B., Marchand, N., Abidi, E., Wiedensohler, A., Drewnick, F.,  
918 Schneider, J., Borrmann, S., Nemitz, E., Zimmermann, R., Jaffrezo, J. L.,  
919 Prevot, A. S. H., and Baltensperger, U.: Wintertime aerosol chemical  
920 composition and source apportionment of the organic fraction in the  
921 metropolitan area of Paris, *Atmo. Chem. Phys.*, 13, 961-981, 2013b.  
922 Crippa, M., Canonaco, F., Lanz, V. A., Aijala, M., Allan, J. D., Carbone, S., Capes,  
923 G., Ceburnis, D., Dall'Osto, M., Day, D. A., DeCarlo, P. F., Ehn, M., Eriksson,  
924 A., Freney, E., Ruiz, L. H., Hillamo, R., Jimenez, J. L., Junninen, H., Kiendler-  
925 Scharr, A., Kortelainen, A. M., Kulmala, M., Laaksonen, A., Mensah, A., Mohr,  
926 C., Nemitz, E., O'Dowd, C., Ovadnevaite, J., Pandis, S. N., Petaja, T., Poulain,

927 L., Saarikoski, S., Sellegri, K., Swietlicki, E., Tiitta, P., Worsnop, D. R.,  
 928 Baltensperger, U., and Prevot, A. S. H.: Organic aerosol components derived  
 929 from 25 AMS data sets across Europe using a consistent ME-2 based source  
 930 apportionment approach, *Atmo. Chem. Phys.*, 14, 2014.

931 DeCarlo, P. F., Ulbrich, I. M., Crounse, J., de Foy, B., Dunlea, E. J., Aiken, A. C.,  
 932 Knapp, D., Weinheimer, A. J., Campos, T., Wennberg, P. O., and Jimenez, J.  
 933 L.: Investigation of the sources and processing of organic aerosol over the  
 934 Central Mexican Plateau from aircraft measurements during MILAGRO, *Atmo.*  
 935 *Chem. Phys.*, 10, 5257-5280, 2010.

936 Denier van der Gon, H. A. C., Bergström, R., Fountoukis, C., Johansson, C., Pandis,  
 937 S. N., Simpson, D., and Visschedijk, A.: Particulate emissions from residential  
 938 wood combustion in Europe – revised estimates and an evaluation, *Atmos.*  
 939 *Chem. Phys. Discuss.*, 14, 31719-31765, 2014.

940 Donahue, N. M., Robinson, A. L., Stanier, C. O., and Pandis, S. N.: Coupled  
 941 partitioning, dilution, and chemical aging of semivolatile organics, *Environ. Sci.*  
 942 *Technol.*, 40, 2635-2643, 2006.

943 Donahue, N. M., Robinson, A. L., and Pandis, S. N.: Atmospheric organic particulate  
 944 matter: From smoke to secondary organic aerosol, *Atmo. Environ.*, 43, 94-106,  
 945 2009.

946 Ehn, M., Thornton, J. A., Kleist, E., Sipila, M., Junninen, H., Pullinen, I., Springer,  
 947 M., Rubach, F., Tillmann, R., Lee, B., Lopez-Hilfiker, F., Andres, S., Acir, I.-  
 948 H., Rissanen, M., Jokinen, T., Schobesberger, S., Kangasluoma, J., Kontkanen,  
 949 J., Nieminen, T., Kurten, T., Nielsen, L. B., Jorgensen, S., Kjaergaard, H. G.,  
 950 Canagaratna, M., Maso, M. D., Berndt, T., Petaja, T., Wahner, A., Kerminen,  
 951 V.-M., Kulmala, M., Worsnop, D. R., Wildt, J., and Mentel, T. F.: A large  
 952 source of low-volatility secondary organic aerosol, *Nature*, 506, doi:  
 953 10.1038/nature13032, 2014.

954 Fountoukis, C., Racherla, P. N., van der Gon, H. A. C. D., Polymeneas, P.,  
 955 Charalampidis, P. E., Pilinis, C., Wiedensohler, A., Dall'Osto, M., O'Dowd, C.,  
 956 and Pandis, S. N.: Evaluation of a three-dimensional chemical transport model  
 957 (PMCAMx) in the European domain during the EUCAARI May 2008  
 958 campaign, *Atmos. Chem. and Phys.*, 11, 10331-10347, 2011.

959 Fountoukis, C., Megaritis, A. G., Skyllakou, K., Charalampidis, P. E., Pilinis, C., van  
 960 der Gon, H., Crippa, M., Canonaco, F., Mohr, C., Prevot, A. S. H., Allan, J. D.,  
 961 Poulain, L., Petaja, T., Tiitta, P., Carbone, S., Kiendler-Scharr, A., Nemitz, E.,  
 962 O'Dowd, C., Swietlicki, E., and Pandis, S. N.: Organic aerosol concentration  
 963 and composition over Europe: insights from comparison of regional model  
 964 predictions with aerosol mass spectrometer factor analysis, *Atmo. Chem. Phys.*,  
 965 14, 9061-9076, 2014.

966 Fountoukis, C., Megaritis, A. G., Skyllakou, K., Charalampidis, P. E., Denier van der  
 967 Gon, H. A. C., Crippa, M., Prévôt, A. S. H., Freutel, F., Wiedensohler, A.,  
 968 Pilinis, C., and Pandis, S. N.: Simulating the formation of carbonaceous aerosol  
 969 in a European Megacity (Paris) during the MEGAPOLI summer and winter  
 970 campaigns, *Atmos. Chem. Phys. Discuss.*, 15, 25547-25582, 2015.

971 Ge, X., Setyan, A., Sun, Y., and Zhang, Q.: Primary and secondary organic aerosols  
 972 in Fresno, California during wintertime: Results from high resolution aerosol  
 973 mass spectrometry, *Journal of Geophysical Research-Atmospheres*, 117,  
 974 10.1029/2012jd018026, 2012.

975 Gentner, D. R., Isaacman, G., Worton, D. R., Chan, A. W. H., Dallmann, T. R., Davis,  
976 L., Liu, S., Day, D. A., Russell, L. M., Wilson, K. R., Weber, R., Guha, A.,  
977 Harley, R. A., and Goldstein, A. H.: Elucidating secondary organic aerosol from  
978 diesel and gasoline vehicles through detailed characterization of organic carbon  
979 emissions, *Proceedings of the National Academy of Sciences of the United*  
980 *States of America*, 109, 18318-18323, 2012.

981 Goldstein, A. H., and Galbally, I. E.: Known and unexplored organic constituents in  
982 the earth's atmosphere, *Environ. Sci. Tech.*, 41, 1514-1521, 2007.

983 Gordon, T. D., Presto, A. A., May, A. A., Nguyen, N. T., Lipsky, E. M., Donahue, N.  
984 M., Gutierrez, A., Zhang, M., Maddox, C., Rieger, P., Chattopadhyay, S.,  
985 Maldonado, H., Maricq, M. M., and Robinson, A. L.: Secondary organic aerosol  
986 formation exceeds primary particulate matter emissions for light-duty gasoline  
987 vehicles, *Atmo. Chem. Phys.*, 14, 2014.

988 Grieshop, A. P., Logue, J. M., Donahue, N. M., and Robinson, A. L.: Laboratory  
989 investigation of photochemical oxidation of organic aerosol from wood fires 1:  
990 measurement and simulation of organic aerosol evolution, *Atmos. Chem. Phys.*,  
991 9, 1263-1277, 2009.

992 Hayes, P. L., Ortega, A. M., Cubison, M. J., Froyd, K. D., Zhao, Y., Cliff, S. S., Hu,  
993 W. W., Toohey, D. W., Flynn, J. H., Lefer, B. L., Grossberg, N., Alvarez, S.,  
994 Rappenglueck, B., Taylor, J. W., Allan, J. D., Holloway, J. S., Gilman, J. B.,  
995 Kuster, W. C., De Gouw, J. A., Massoli, P., Zhang, X., Liu, J., Weber, R. J.,  
996 Corrigan, A. L., Russell, L. M., Isaacman, G., Worton, D. R., Kreisberg, N. M.,  
997 Goldstein, A. H., Thalman, R., Waxman, E. M., Volkamer, R., Lin, Y. H.,  
998 Surratt, J. D., Kleindienst, T. E., Offenberg, J. H., Dusanter, S., Griffith, S.,  
999 Stevens, P. S., Brioude, J., Angevine, W. M., and Jimenez, J. L.: Organic  
1000 aerosol composition and sources in Pasadena, California, during the 2010  
1001 CalNex campaign, *J. Geophys. Res. Atmo.*, 118, 9233-9257, doi:  
1002 10.1002/jgrd.50530, 2013.

1003 Henze, D. K., Seinfeld, J. H., Ng, N. L., Kroll, J. H., Fu, T. M., Jacob, D. J., and  
1004 Heald, C. L.: Global modeling of secondary organic aerosol formation from  
1005 aromatic hydrocarbons: high- vs. low-yield pathways, *Atmo. Chem. Phys.*, 8,  
1006 2405-2420, 2008.

1007 Hodzic, A., Jimenez, J. L., Madronich, S., Canagaratna, M. R., DeCarlo, P. F.,  
1008 Kleinman, L., and Fast, J.: Modeling organic aerosols in a megacity: potential  
1009 contribution of semi-volatile and intermediate volatility primary organic  
1010 compounds to secondary organic aerosol formation, *Atmos. Chem. Phys.*, 10,  
1011 5491-5514, 2010.

1012 Hodzic, A., Kasibhatla, P. S., Jo, D. S., Cappa, C., Jimenez, J. L., Madronich, S., and  
1013 Park, R. J.: Rethinking the global secondary organic aerosol (SOA) budget:  
1014 stronger production, faster removal, shorter lifetime, *Atmos. Chem. Phys.*  
1015 *Discuss.*, 2015, 32413-32468, 10.5194/acpd-15-32413-2015, 2015.

1016 Hu, W. W., Campuzano-Jost, P., Palm, B. B., Day, D. A., Ortega, A. M., Hayes, P. L.,  
1017 Krechmer, J. E., Chen, Q., Kuwata, M., Liu, Y. J., de Sa, S. S., McKinney, K.,  
1018 Martin, S. T., Hu, M., Budisulistiorini, S. H., Riva, M., Surratt, J. D., St Clair, J.  
1019 M., Isaacman-Van Wertz, G., Yee, L. D., Goldstein, A. H., Carbone, S., Brito,  
1020 J., Artaxo, P., de Gouw, J. A., Koss, A., Wisthaler, A., Mikoviny, T., Karl, T.,  
1021 Kaser, L., Jud, W., Hansel, A., Docherty, K. S., Alexander, M. L., Robinson, N.  
1022 H., Coe, H., Allan, J. D., Canagaratna, M. R., Paulot, F., and Jimenez, J. L.:  
1023 Characterization of a real-time tracer for isoprene epoxydiols-derived secondary

1024 organic aerosol (IEPOX-SOA) from aerosol mass spectrometer measurements,  
1025 Atmospheric Chemistry and Physics, 15, 11807-11833, 10.5194/acp-15-11807-  
1026 2015, 2015.

1027 IPCC: (Intergovernmental Panel on Climate Change): The physical science basis.  
1028 Contribution of working group I to the fifth assessment report of the  
1029 intergovernmental panel on climate change. T.F. Stocker, D. Qin, G.-K.  
1030 Plattner, M. Tignor, S.K. Allen, J. Boschung, A. Nauels, Y. Xia, V. Bex, and  
1031 P.M. Midgley (eds.). Cambridge University Press, Cambridge, United Kingdom  
1032 and New York, NY, USA, 2013.

1033 Jathar, S. H., Farina, S. C., Robinson, A. L., and Adams, P. J.: The influence of semi-  
1034 volatile and reactive primary emissions on the abundance and properties of  
1035 global organic aerosol, *Atmos. Chem. Phys.*, 11, 7727-7746, 2011.

1036 Jimenez, J. L., Jayne, J. T., Shi, Q., Kolb, C. E., Worsnop, D. R., Yourshaw, I.,  
1037 Seinfeld, J. H., Flagan, R. C., Zhang, X. F., Smith, K. A., Morris, J. W., and  
1038 Davidovits, P.: Ambient aerosol sampling using the Aerodyne Aerosol Mass  
1039 Spectrometer, *J. Geophys. Res. Atmos.*, 108, doi: 10.1029/2001jd001213, 2003.

1040 Jimenez, J. L., Canagaratna, M. R., Donahue, N. M., Prevot, A. S. H., Zhang, Q.,  
1041 Kroll, J. H., DeCarlo, P. F., Allan, J. D., Coe, H., Ng, N. L., Aiken, A. C.,  
1042 Docherty, K. S., Ulbrich, I. M., Grieshop, A. P., Robinson, A. L., Duplissy, J.,  
1043 Smith, J. D., Wilson, K. R., Lanz, V. A., Hueglin, C., Sun, Y. L., Tian, J.,  
1044 Laaksonen, A., Raatikainen, T., Rautiainen, J., Vaattovaara, P., Ehn, M.,  
1045 Kulmala, M., Tomlinson, J. M., Collins, D. R., Cubison, M. J., Dunlea, E. J.,  
1046 Huffman, J. A., Onasch, T. B., Alfarra, M. R., Williams, P. I., Bower, K.,  
1047 Kondo, Y., Schneider, J., Drewnick, F., Borrmann, S., Weimer, S., Demerjian,  
1048 K., Salcedo, D., Cottrell, L., Griffin, R., Takami, A., Miyoshi, T., Hatakeyama,  
1049 S., Shimo, A., Sun, J. Y., Zhang, Y. M., Dzepina, K., Kimmel, J. R., Sueper,  
1050 D., Jayne, J. T., Herndon, S. C., Trimborn, A. M., Williams, L. R., Wood, E. C.,  
1051 Middlebrook, A. M., Kolb, C. E., Baltensperger, U., and Worsnop, D. R.:  
1052 Evolution of organic aerosols in the atmosphere, *Science*, 326, 1525-1529,  
1053 2009.

1054 Jöckel, P., Tost, H., Pozzer, A., Bruehl, C., Buchholz, J., Ganzeveld, L., Hoor, P.,  
1055 Kerkweg, A., Lawrence, M. G., Sander, R., Steil, B., Stiller, G., Tanarhte, M.,  
1056 Taraborrelli, D., Van Aardenne, J., and Lelieveld, J.: The atmospheric chemistry  
1057 general circulation model ECHAM5/MESy1: consistent simulation of ozone  
1058 from the surface to the mesosphere, *Atmos. Chem. Phys.*, 6, 5067-5104, 2006.

1059 Kanakidou, M., Seinfeld, J. H., Pandis, S. N., Barnes, I., Dentener, F. J., Facchini, M.  
1060 C., Van Dingenen, R., Ervens, B., Nenes, A., Nielsen, C. J., Swietlicki, E.,  
1061 Putaud, J. P., Balkanski, Y., Fuzzi, S., Horth, J., Moortgat, G. K., Winterhalter,  
1062 R., Myhre, C. E. L., Tsigaridis, K., Vignati, E., Stephanou, E. G., and Wilson,  
1063 J.: Organic aerosol and global climate modelling: a review, *Atmos. Chem.  
1064 Phys.*, 5, 1053-1123, 2005.

1065 Karydis, V. A., Tsimpidi, A. P., Pozzer, A., Astitha, M., and Lelieveld, J.: Effects of  
1066 mineral dust on global atmospheric nitrate concentrations, *Atmos. Chem. Phys.*,  
1067 16, 1491-1509, 10.5194/acp-16-1491-2016, 2016.

1068 Kerkweg, A., Buchholz, J., Ganzeveld, L., Pozzer, A., Tost, H., and Jöckel, P.:  
1069 Technical Note: An implementation of the dry removal processes DRY  
1070 DEPosition and SEDimentation in the Modular Earth Submodel System  
1071 (MESSy), *Atmos. Chem. Phys.*, 6, 4617-4632, 2006a.

1072 Kerkweg, A., Sander, R., Tost, H., and Jöckel, P.: Technical note: Implementation of  
1073 prescribed (OFFLEM), calculated (ONLEM), and pseudo-emissions  
1074 (TNUDGE) of chemical species in the Modular Earth Submodel System  
1075 (MESSy), *Atmos. Chem. Phys.*, 6, 3603-3609, 2006b.

1076 Kopacz, M., Jacob, D. J., Fisher, J. A., Logan, J. A., Zhang, L., Megretskaja, I. A.,  
1077 Yantosca, R. M., Singh, K., Henze, D. K., Burrows, J. P., Buchwitz, M.,  
1078 Khlystova, I., McMillan, W. W., Gille, J. C., Edwards, D. P., Eldering, A.,  
1079 Thouret, V., and Nedelec, P.: Global estimates of CO sources with high  
1080 resolution by adjoint inversion of multiple satellite datasets (MOPITT, AIRS,  
1081 SCIAMACHY, TES), *Atmos. Chem. Phys.*, 10, 855-876, 10.5194/acp-10-855-  
1082 2010, 2010.

1083 Kostenidou, E., Kaltsonoudis, C., Tsiflikiotou, M., Louvaris, E., Russell, L. M., and  
1084 Pandis, S. N.: Burning of olive tree branches: a major organic aerosol source in  
1085 the Mediterranean, *Atmo. Chem. Phys.*, 13, 8797-8811, 2013.

1086 Kroll, J. H., and Seinfeld, J. H.: Chemistry of secondary organic aerosol: Formation  
1087 and evolution of low-volatility organics in the atmosphere, *Atmos. Environ.*, 42,  
1088 3593-3624, 2008.

1089 Lanz, V. A., Alfarra, M. R., Baltensperger, U., Buchmann, B., Hueglin, C., and  
1090 Prevot, A. S. H.: Source apportionment of submicron organic aerosols at an  
1091 urban site by factor analytical modelling of aerosol mass spectra, *Atmo. Chem.*  
1092 *Phys.*, 7, 1503-1522, 2007.

1093 Lanz, V. A., Alfarra, M. R., Baltensperger, U., Buchmann, B., Hueglin, C., Szidat, S.,  
1094 Wehrli, M. N., Wacker, L., Weimer, S., Caseiro, A., Puxbaum, H., and Prevot,  
1095 A. S. H.: Source attribution of submicron organic aerosols during wintertime  
1096 inversions by advanced factor analysis of aerosol mass spectra, *Environ. Sci.*  
1097 *Tech.*, 42, 214-220, 2008.

1098 Lanz, V. A., Prevot, A. S. H., Alfarra, M. R., Weimer, S., Mohr, C., DeCarlo, P. F.,  
1099 Gianini, M. F. D., Hueglin, C., Schneider, J., Favez, O., D'Anna, B., George, C.,  
1100 and Baltensperger, U.: Characterization of aerosol chemical composition with  
1101 aerosol mass spectrometry in Central Europe: an overview, *Atmo. Chem. Phys.*,  
1102 10, 10453-10471, 2010.

1103 Lauer, A., Eyring, V., Hendricks, J., Joeckel, P., and Lohmann, U.: Global model  
1104 simulations of the impact of ocean-going ships on aerosols, clouds, and the  
1105 radiation budget, *Atmos. Chem. Phys.*, 7, 5061-5079, 2007.

1106 Lee, L. A., Pringle, K. J., Reddington, C. L., Mann, G. W., Stier, P., Spracklen, D. V.,  
1107 Pierce, J. R., and Carslaw, K. S.: The magnitude and causes of uncertainty in  
1108 global model simulations of cloud condensation nuclei, *Atmos. Chem. Phys.*,  
1109 13, 8879-8914, 2013.

1110 Lelieveld, J., Barlas, C., Giannadaki, D., and Pozzer, A.: Model calculated global,  
1111 regional and megacity premature mortality due to air pollution, *Atmos. Chem.*  
1112 *Phys.*, 13, 7023-7037, 2013.

1113 Lelieveld, J., Evans, J. S., Fnais, M., Giannadaki, D., and Pozzer, A.: The contribution  
1114 of outdoor air pollution sources to premature mortality on a global scale,  
1115 *Nature*, 525, 367-+, 10.1038/nature15371, 2015.

1116 Marcolli, C., Canagaratna, M. R., Worsnop, D. R., Bahreini, R., de Gouw, J. A.,  
1117 Warneke, C., Goldan, P. D., Kuster, W. C., Williams, E. J., Lerner, B. M.,  
1118 Roberts, J. M., Meagher, J. F., Fehsenfeld, F. C., Marchewka, M., Bertman, S.  
1119 B., and Middlebrook, A. M.: Cluster analysis of the organic peaks in bulk mass



1120 spectra obtained during the 2002 New England air quality study with an  
1121 Aerodyne aerosol mass spectrometer, *Atmo. Chem. Phys.*, 6, 5649-5666, 2006.

1122 May, A. A., Levin, E. J. T., Hennigan, C. J., Riipinen, I., Lee, T., Collett, J. L.,  
1123 Jimenez, J. L., Kreidenweis, S. M., and Robinson, A. L.: Gas-particle  
1124 partitioning of primary organic aerosol emissions: 3. Biomass burning, *J.*  
1125 *Geophys. Res. Atmo.*, 118, 11327-11338, doi: 10.1002/jgrd.50828, 2013.

1126 May, A. A., Nguyen, N. T., Presto, A. A., Gordon, T. D., Lipsky, E. M., Karve, M.,  
1127 Gutierrez, A., Robertson, W. H., Zhang, M., Brandow, C., Chang, O., Chen, S.,  
1128 Cicero-Fernandez, P., Dinkins, L., Fuentes, M., Huang, S.-M., Ling, R., Long,  
1129 J., Maddox, C., Massetti, J., McCauley, E., Miguel, A., Na, K., Ong, R., Pang,  
1130 Y., Rieger, P., Sax, T., Tin, T., Thu, V., Chattopadhyay, S., Maldonado, H.,  
1131 Maricq, M. M., and Robinson, A. L.: Gas- and particle-phase primary emissions  
1132 from in-use, on-road gasoline and diesel vehicles, *Atmospheric Environment*,  
1133 88, 247-260, 10.1016/j.atmosenv.2014.01.046, 2014.

1134 McFiggans, G., Artaxo, P., Baltensperger, U., Coe, H., Facchini, M. C., Feingold, G.,  
1135 Fuzzi, S., Gysel, M., Laaksonen, A., Lohmann, U., Mentel, T. F., Murphy, D.  
1136 M., O'Dowd, C. D., Snider, J. R., and Weingartner, E.: The effect of physical  
1137 and chemical aerosol properties on warm cloud droplet activation, *Atmo. Chem.*  
1138 *Phys.*, 6, 2593-2649, 2006.

1139 Miracolo, M. A., Hennigan, C. J., Ranjan, M., Nguyen, N. T., Gordon, T. D., Lipsky,  
1140 E. M., Presto, A. A., Donahue, N. M., and Robinson, A. L.: Secondary aerosol  
1141 formation from photochemical aging of aircraft exhaust in a smog chamber,  
1142 *Atmo. Chem. Phys.*, 11, 4135-4147, 2011.

1143 Mohr, C., DeCarlo, P. F., Heringa, M. F., Chirico, R., Slowik, J. G., Richter, R.,  
1144 Reche, C., Alastuey, A., Querol, X., Seco, R., Penuelas, J., Jimenez, J. L.,  
1145 Crippa, M., Zimmermann, R., Baltensperger, U., and Prevot, A. S. H.:  
1146 Identification and quantification of organic aerosol from cooking and other  
1147 sources in Barcelona using aerosol mass spectrometer data, *Atmo. Chem. Phys.*,  
1148 12, 1649-1665, 2012.

1149 Murphy, B. N., and Pandis, S. N.: Simulating the formation of semivolatile primary  
1150 and secondary organic aerosol in a regional chemical transport model, *Environ.*  
1151 *Sci. Technol.*, 43, 4722-4728, 2009.

1152 Nemitz, E., Jimenez, J. L., Huffman, J. A., Ulbrich, I. M., Canagaratna, M. R.,  
1153 Worsnop, D. R., and Guenther, A. B.: An eddy-covariance system for the  
1154 measurement of surface/atmosphere exchange fluxes of submicron aerosol  
1155 chemical species - First application above an urban area, *Aerosol Sci. Tech.*, 42,  
1156 636-657, 2008.

1157 Ng, N. L., Canagaratna, M. R., Jimenez, J. L., Zhang, Q., Ulbrich, I. M., and  
1158 Worsnop, D. R.: Real-Time Methods for Estimating Organic Component Mass  
1159 Concentrations from Aerosol Mass Spectrometer Data, *Environ. Sci. Tech.*, 45,  
1160 910-916, 2011.

1161 Paatero, P., and Tapper, U.: Positive matrix factorization-A nonnegative factor model  
1162 with optimal utilization of error-estimates of data values, *Environmetrics*, 5,  
1163 111-126, 1994.

1164 Paatero, P.: Least squares formulation of robust non-negative factor analysis,  
1165 *Chemometrics and Intelligent Laboratory Systems*, 37, 23-35, 1997.

1166 Poschl, U.: Atmospheric aerosols: Composition, transformation, climate and health  
1167 effects, *Angew. Chem.-Int. Edit.*, 44, 7520-7540, 2005.

1168 Pozzer, A., Zimmermann, P., Doering, U. M., van Aardenne, J., Tost, H., Dentener,  
1169 F., Janssens-Maenhout, G., and Lelieveld, J.: Effects of business-as-usual  
1170 anthropogenic emissions on air quality, *Atmos. Chem. Phys.*, 12, 6915-6937,  
1171 10.5194/acp-12-6915-2012, 2012a.

1172 Pozzer, A., de Meij, A., Pringle, K. J., Tost, H., Doering, U. M., van Aardenne, J., and  
1173 Lelieveld, J.: Distributions and regional budgets of aerosols and their precursors  
1174 simulated with the EMAC chemistry-climate model, *Atmos. Chem. Phys.*, 12,  
1175 961-987, 2012b.

1176 Pringle, K. J., Tost, H., Message, S., Steil, B., Giannadaki, D., Nenes, A., Fountoukis,  
1177 C., Stier, P., Vignati, E., and Lelieveld, J.: Description and evaluation of GMXc:  
1178 a new aerosol submodel for global simulations (v1), *Geoscientific Model  
1179 Development*, 3, 391-412, 2010.

1180 Pye, H. O. T., and Seinfeld, J. H.: A global perspective on aerosol from low-volatility  
1181 organic compounds, *Atmos. Chem. Phys.*, 10, 4377-4401, 2010.

1182 Ranjan, M., Presto, A. A., May, A. A., and Robinson, A. L.: Temperature  
1183 Dependence of Gas-Particle Partitioning of Primary Organic Aerosol Emissions  
1184 from a Small Diesel Engine, *Aerosol Science and Technology*, 46, 13-21,  
1185 10.1080/02786826.2011.602761, 2012.

1186 Robinson, A. L., Donahue, N. M., Shrivastava, M. K., Weitkamp, E. A., Sage, A. M.,  
1187 Grieshop, A. P., Lane, T. E., Pierce, J. R., and Pandis, S. N.: Rethinking organic  
1188 aerosols: Semivolatile emissions and photochemical aging, *Science*, 315, 1259-  
1189 1262, 2007.

1190 Robinson, A. L., Grieshop, A. P., Donahue, N. M., and Hunt, S. W.: Updating the  
1191 conceptual model for fine particle mass emissions from combustion systems, *J.  
1192 Air Waste Manage.*, 60, 1204-1222, 2010.

1193 Samy, S., and Zielinska, B.: Secondary organic aerosol production from modern  
1194 diesel engine emissions, *Atmos. Chem. Phys.*, 10, 609-625, 2010.

1195 Sander, R., Baumgaertner, A., Gromov, S., Harder, H., Joeckel, P., Kerckweg, A.,  
1196 Kubistin, D., Regelin, E., Riede, H., Sandu, A., Taraborrelli, D., Tost, H., and  
1197 Xie, Z. Q.: The atmospheric chemistry box model CAABA/MECCA-3.0,  
1198 *Geoscientific Model Development*, 4, 373-380, 2011.

1199 Shrivastava, M. K., Lane, T. E., Donahue, N. M., Pandis, S. N., and Robinson, A. L.:  
1200 Effects of gas particle partitioning and aging of primary emissions on urban and  
1201 regional organic aerosol concentrations, *J. Geophys. Res. Atmos.*, 113, doi:  
1202 10.1029/2007jd009735, 2008.

1203 Shrivastava, M., Fast, J., Easter, R., Gustafson, W. I., Jr., Zaveri, R. A., Jimenez, J. L.,  
1204 Saide, P., and Hodzic, A.: Modeling organic aerosols in a megacity: comparison  
1205 of simple and complex representations of the volatility basis set approach,  
1206 *Atmos. Chem. Phys.*, 11, 6639-6662, 2011.

1207 Shrivastava, M., Easter, R. C., Liu, X., Zelenyuk, A., Singh, B., Zhang, K., Ma, P.-L.,  
1208 Chand, D., Ghan, S., Jimenez, J. L., Zhang, Q., Fast, J., Rasch, P. J., and Tiitta,  
1209 P.: Global transformation and fate of SOA: Implications of low-volatility SOA  
1210 and gas-phase fragmentation reactions, *Journal of Geophysical Research:  
1211 Atmospheres*, 120, 4169-4195, 10.1002/2014JD022563, 2015.

1212 Spracklen, D. V., Jimenez, J. L., Carslaw, K. S., Worsnop, D. R., Evans, M. J., Mann,  
1213 G. W., Zhang, Q., Canagaratna, M. R., Allan, J., Coe, H., McFiggans, G., Rap,  
1214 A., and Forster, P.: Aerosol mass spectrometer constraint on the global  
1215 secondary organic aerosol budget, *Atmos. Chem. Phys.*, 11, 12109-12136, 2011.

1216 Stone, E. A., Zhou, J., Snyder, D. C., Rutter, A. P., Mieritz, M., and Schauer, J. J.: A  
1217 Comparison of Summertime Secondary Organic Aerosol Source Contributions  
1218 at Contrasting Urban Locations, *Environ. Sci. Tech.*, 43, 3448-3454, 2009.

1219 Stubenrauch, C. J., Chedin, A., Radel, G., Scott, N. A., and Serrar, S.: Cloud  
1220 properties and their seasonal and diurnal variability from TOVS path-B, *Journal*  
1221 *of Climate*, 19, 5531-5553, 10.1175/jcli3929.1, 2006.

1222 Suess, D. T., and Prather, K. A.: Mass spectrometry of aerosols, *Chemical Reviews*,  
1223 99, 3007-+, 1999.

1224 Sun, Y. L., Zhang, Q., Schwab, J. J., Demerjian, K. L., Chen, W. N., Bae, M. S.,  
1225 Hung, H. M., Hogrefe, O., Frank, B., Rattigan, O. V., and Lin, Y. C.:  
1226 Characterization of the sources and processes of organic and inorganic aerosols  
1227 in New York city with a high-resolution time-of-flight aerosol mass  
1228 spectrometer, *Atmospheric Chemistry and Physics*, 11, 1581-1602,  
1229 10.5194/acp-11-1581-2011, 2011.

1230 Takegawa, N., Miyazaki, Y., Kondo, Y., Komazaki, Y., Miyakawa, T., Jimenez, J. L.,  
1231 Jayne, J. T., Worsnop, D. R., Allan, J. D., and Weber, R. J.: Characterization of  
1232 an Aerodyne Aerosol Mass Spectrometer (AMS): Intercomparison with other  
1233 aerosol instruments, *Aerosol Sci. Tech.*, 39, 760-770, 2005.

1234 Tost, H., Jockel, P. J., Kerkweg, A., Sander, R., and Lelieveld, J.: Technical note: A  
1235 new comprehensive SCAVenging submodel for global atmospheric chemistry  
1236 modelling, *Atmos. Chem. Phys.*, 6, 565-574, 2006.

1237 Tsigaridis, K., Daskalakis, N., Kanakidou, M., Adams, P. J., Artaxo, P., Bahadur, R.,  
1238 Balkanski, Y., Bauer, S. E., Bellouin, N., Benedetti, A., Bergman, T., Berntsen,  
1239 T. K., Beukes, J. P., Bian, H., Carslaw, K. S., Chin, M., Curci, G., Diehl, T.,  
1240 Easter, R. C., Ghan, S. J., Gong, S. L., Hodzic, A., Hoyle, C. R., Iversen, T.,  
1241 Jathar, S., Jimenez, J. L., Kaiser, J. W., Kirkevag, A., Koch, D., Kokkola, H.,  
1242 Lee, Y. H., Lin, G., Liu, X., Luo, G., Ma, X., Mann, G. W., Mihalopoulos, N.,  
1243 Morcrette, J. J., Mueller, J. F., Myhre, G., Myriokefalitakis, S., Ng, N. L.,  
1244 O'Donnell, D., Penner, J. E., Pozzoli, L., Pringle, K. J., Russell, L. M., Schulz,  
1245 M., Sciare, J., Seland, O., Shindell, D. T., Sillman, S., Skeie, R. B., Spracklen,  
1246 D., Stavrou, T., Steenrod, S. D., Takemura, T., Tiitta, P., Tilmes, S., Tost, H.,  
1247 van Noije, T., van Zyl, P. G., von Salzen, K., Yu, F., Wang, Z., Wang, Z.,  
1248 Zaveri, R. A., Zhang, H., Zhang, K., Zhang, Q., and Zhang, X.: The AeroCom  
1249 evaluation and intercomparison of organic aerosol in global models, *Atmo.*  
1250 *Chem. Phys.*, 14, 10845-10895, 2014.

1251 Tsimpidi, A. P., Karydis, V. A., Zavala, M., Lei, W., Molina, L., Ulbrich, I. M.,  
1252 Jimenez, J. L., and Pandis, S. N.: Evaluation of the volatility basis-set approach  
1253 for the simulation of organic aerosol formation in the Mexico City metropolitan  
1254 area, *Atmos. Chem. Phys.*, 10, 525-546, 2010.

1255 Tsimpidi, A. P., Karydis, V. A., Zavala, M., Lei, W., Bei, N., Molina, L., and Pandis,  
1256 S. N.: Sources and production of organic aerosol in Mexico City: insights from  
1257 the combination of a chemical transport model (PMCAMx-2008) and  
1258 measurements during MILAGRO, *Atmos. Chem. Phys.*, 11, 5153-5168, 2011.

1259 Tsimpidi, A. P., Karydis, V. A., Pozzer, A., Pandis, S. N., and Lelieveld, J.: ORACLE  
1260 (v1.0): module to simulate the organic aerosol composition and evolution in the  
1261 atmosphere, *Geoscientific Model Development*, 7, 3153-3172, 2014.

1262 Ulbrich, I. M., Canagaratna, M. R., Zhang, Q., Worsnop, D. R., and Jimenez, J. L.:  
1263 Interpretation of organic components from Positive Matrix Factorization of  
1264 aerosol mass spectrometric data, *Atmo. Chem. Phys.*, 9, 2891-2918, 2009.

1265 van der Werf, G. R., Randerson, J. T., Giglio, L., Collatz, G. J., Mu, M., Kasibhatla,  
1266 P. S., Morton, D. C., DeFries, R. S., Jin, Y., and van Leeuwen, T. T.: Global fire  
1267 emissions and the contribution of deforestation, savanna, forest, agricultural,  
1268 and peat fires (1997-2009), *Atmos. Chem. Phys.*, 10, 11707-11735, 2010.

1269 Wang, Q., Shao, M., Liu, Y., William, K., Paul, G., Li, X., Liu, Y., and Lu, S.: Impact  
1270 of biomass burning on urban air quality estimated by organic tracers:  
1271 Guangzhou and Beijing as cases, *Atmo. Environ.*, 41, 8380-8390, doi:  
1272 10.1016/j.atmosenv.2007.06.048, 2007.

1273 Weilenmann, M., Favez, J.-Y., and Alvarez, R.: Cold-start emissions of modern  
1274 passenger cars at different low ambient temperatures and their evolution over  
1275 vehicle legislation categories, *Atmos. Environ.*, 43, 2419-2429, 2009.

1276 Westerholm, R., Christensen, A., and Rosen, A.: Regulated and unregulated exhaust  
1277 emissions from two three-way catalyst equipped gasoline fuelled vehicles,  
1278 *Atmos. Environ.*, 30, 3529-3536, 1996.

1279 Zhang, Q., Alfarra, M. R., Worsnop, D. R., Allan, J. D., Coe, H., Canagaratna, M. R.,  
1280 and Jimenez, J. L.: Deconvolution and quantification of hydrocarbon-like and  
1281 oxygenated organic aerosols based on aerosol mass spectrometry, *Environ. Sci.*  
1282 *Tech.*, 39, 4938-4952, 2005a.

1283 Zhang, Q., Canagaratna, M. R., Jayne, J. T., Worsnop, D. R., and Jimenez, J. L.:  
1284 Time- and size-resolved chemical composition of submicron particles in  
1285 Pittsburgh: Implications for aerosol sources and processes, *J. Geophys. Res.-*  
1286 *Atmos.*, 110, doi: 10.1029/2004jd004649, 2005b.

1287 Zhang, Q., Jimenez, J. L., Canagaratna, M. R., Allan, J. D., Coe, H., Ulbrich, I.,  
1288 Alfarra, M. R., Takami, A., Middlebrook, A. M., Sun, Y. L., Dzepina, K.,  
1289 Dunlea, E., Docherty, K., DeCarlo, P. F., Salcedo, D., Onasch, T., Jayne, J. T.,  
1290 Miyoshi, T., Shimo, A., Hatakeyama, S., Takegawa, N., Kondo, Y.,  
1291 Schneider, J., Drewnick, F., Borrmann, S., Weimer, S., Demerjian, K.,  
1292 Williams, P., Bower, K., Bahreini, R., Cottrell, L., Griffin, R. J., Rautiainen, J.,  
1293 Sun, J. Y., Zhang, Y. M., and Worsnop, D. R.: Ubiquity and dominance of  
1294 oxygenated species in organic aerosols in anthropogenically-influenced  
1295 Northern Hemisphere midlatitudes, *Geophys. Res. Lett.*, 34, doi:  
1296 10.1029/2007gl029979, 2007.

1297 Zhang, Q., Jimenez, J. L., Canagaratna, M. R., Ulbrich, I. M., Ng, N. L., Worsnop, D.  
1298 R., and Sun, Y. L.: Understanding atmospheric organic aerosols via factor  
1299 analysis of aerosol mass spectrometry: a review, *Anal. Bioanal. Chem.*, 401,  
1300 3045-3067, 2011.

1301 Zhang, Q. J., Beekmann, M., Drewnick, F., Freutel, F., Schneider, J., Crippa, M.,  
1302 Prevot, A. S. H., Baltensperger, U., Poulain, L., Wiedensohler, A., Sciare, J.,  
1303 Gros, V., Borbon, A., Colomb, A., Michoud, V., Doussin, J. F., van der Gon, H.  
1304 A. C. D., Haeffelin, M., Dupont, J. C., Siour, G., Petetin, H., Bessagnet, B.,  
1305 Pandis, S. N., Hodzic, A., Sanchez, O., Honore, C., and Perrussel, O.:  
1306 Formation of organic aerosol in the Paris region during the MEGAPOLI  
1307 summer campaign: evaluation of the volatility-basis-set approach within the  
1308 CHIMERE model, *Atmos. Chem. Phys.*, 13, 5767-5790, 2013.

1309

1310

1311

1312

1313 **Table 1.** Predicted tropospheric burden in Tg of organic aerosol components during the  
1314 decade 2001-2010.

<b>OA component</b>	<b>Tropospheric burden (Tg)</b>	<b>Monthly Standard Deviation (<math>\sigma</math>)</b>
fPOA	0.06	0.01
fSOA	0.57	0.06
bbPOA	0.18	0.13
bbSOA	0.42	0.27
aSOA	0.44	0.08
bSOA	0.31	0.10
OA	1.98	0.54

1315

1316 **Table 2.** Statistical evaluation of EMAC results against AMS measurements over  
 1317 urban locations of the Northern Hemisphere during 2001-2010.  
 1318

<b>EMAC Element</b>	<b>AMS Element</b>	<b>Number of datasets</b>	<b>Mean Observed (<math>\mu\text{g m}^{-3}</math>)</b>	<b>Mean Predicted (<math>\mu\text{g m}^{-3}</math>)</b>	<b>MAGE (<math>\mu\text{g m}^{-3}</math>)</b>	<b>MB (<math>\mu\text{g m}^{-3}</math>)</b>	<b>NME (%)</b>	<b>NMB (%)</b>	<b>RMSE (<math>\mu\text{g m}^{-3}</math>)</b>
POA*	HOA+BBOA	23	2.70	0.98	1.73	-1.72	64	-64	2.58
SOA	OOA	23	4.25	2.85	1.97	-1.40	46	-33	2.50
Aged SOA	LV-OOA	10	3.43	2.72	1.47	-0.72	43	-21	2.04
Fresh SOA	SV-OOA	10	2.14	1.88	0.69	-0.26	32	-12	0.81

1319

1320 \* Sum of fPOA and bbPOA

1321

1322 **Table 3.** Statistical evaluation of EMAC POA (sum of fPOA and bbPOA) against  
 1323 AMS POA (sum of HOA and BBOA) in the Northern Hemisphere during 2001-2010.

1324

<b>Site Type<sup>a</sup></b>	<b>Number of datasets</b>	<b>Mean Observed</b> ( $\mu\text{g m}^{-3}$ )	<b>Mean Predicted</b> ( $\mu\text{g m}^{-3}$ )	<b>MAGE</b> ( $\mu\text{g m}^{-3}$ )	<b>MB</b> ( $\mu\text{g m}^{-3}$ )	<b>NME</b> (%)	<b>NMB</b> (%)	<b>RMSE</b> ( $\mu\text{g m}^{-3}$ )
Urban Downwind	15	0.82	0.64	0.38	-0.18	47	-22	0.50
Rural/Remote	46	0.43	0.47	0.37	0.04	87	9	0.5
<b>Continent<sup>b</sup></b>								
Europe	42	0.61	0.47	0.36	-0.14	59	-23	0.47
N. America	10	0.51	0.50	0.29	-0.01	57	-3	0.37
Asia	9	0.15	0.69	0.54	0.54	363	363	0.72
<b>Season<sup>c</sup></b>								
Winter	6	1.18	0.74	0.60	-0.44	51	-37	0.76
Spring	30	0.42	0.53	0.41	0.11	97	26	0.52
Summer	14	0.50	0.44	0.30	-0.06	59	-13	0.39
Autumn	11	0.49	0.42	0.27	-0.07	54	-15	0.37
<b>Total</b>	<b>61</b>	<b>0.53</b>	<b>0.51</b>	<b>0.38</b>	<b>-0.02</b>	<b>71</b>	<b>-3</b>	<b>0.50</b>

1325 <sup>a</sup> Statistics are calculated for a specific site type during all seasons

1326 <sup>b</sup> Statistics are calculated for a specific continent excluding the values from urban areas

1327 <sup>c</sup> Statistics are calculated for a specific season excluding the values from urban areas

1328

1329 **Table 4.** Statistical evaluation of EMAC SOA against AMS OOA in the Northern  
 1330 Hemisphere during 2001-2010.

1331

<b>Site Type<sup>a</sup></b>	<b>Number of datasets</b>	<b>Mean Observed</b> ( $\mu\text{g m}^{-3}$ )	<b>Mean Predicted</b> ( $\mu\text{g m}^{-3}$ )	<b>MAGE</b> ( $\mu\text{g m}^{-3}$ )	<b>MB</b> ( $\mu\text{g m}^{-3}$ )	<b>NME</b> (%)	<b>NMB</b> (%)	<b>RMSE</b> ( $\mu\text{g m}^{-3}$ )
Urban Downwind	15	2.98	2.07	1.20	-0.91	40	-30	1.77
Rural/Remote	46	2.72	1.86	1.45	-0.86	54	-32	2.09
<b>Continent<sup>b</sup></b>								
Europe	42	2.47	1.49	1.59	-0.98	64	-39	2.28
N. America	10	3.29	2.78	0.91	-0.51	28	-15	1.37
Asia	9	3.68	2.89	1.00	-0.79	27	-22	1.11
<b>Season<sup>c</sup></b>								
Winter	6	2.81	0.50	2.31	-2.31	82	-82	2.65
Spring	30	2.22	1.79	0.97	-0.43	44	-20	1.18
Summer	14	4.30	2.89	2.04	-1.41	47	-33	3.20
Autumn	11	2.35	1.78	1.22	-0.57	52	-25	1.39
<b>Total</b>	61	2.78	1.91	1.39	-0.87	50	-31	2.02

1332 <sup>a</sup> Statistics are calculated for a specific site type during all four seasons

1333 <sup>b</sup> Statistics are calculated for a specific continent excluding the values from urban areas

1334 <sup>c</sup> Statistics are calculated for a specific season excluding the values from urban areas

1335



1336 **Table 5.** Statistical evaluation of EMAC aged SOA against AMS LV-OOA in the  
 1337 Northern Hemisphere during 2001-2010.

1338

<b>Site Type<sup>a</sup></b>	<b>Number of datasets</b>	<b>Mean Observed</b> ( $\mu\text{g m}^{-3}$ )	<b>Mean Predicted</b> ( $\mu\text{g m}^{-3}$ )	<b>MAGE</b> ( $\mu\text{g m}^{-3}$ )	<b>MB</b> ( $\mu\text{g m}^{-3}$ )	<b>NME</b> (%)	<b>NMB</b> (%)	<b>RMSE</b> ( $\mu\text{g m}^{-3}$ )
Urban Downwind	8	1.77	0.94	1.28	-0.83	72	-47	1.55
Rural/Remote	33	1.65	1.02	1.17	-0.63	71	-38	1.69
<b>Continent<sup>b</sup></b>								
Europe	35	1.71	0.98	1.24	-0.73	73	-43	0.47
N. America	6	1.45	1.17	0.87	-0.28	60	-20	1.00
Asia	-	-	-	-	-	-	-	-
<b>Season<sup>c</sup></b>								
Winter	3	2.36	0.20	2.16	-2.16	91	-91	2.36
Spring	18	1.06	0.81	0.82	-0.25	77	-24	1.03
Summer	11	2.64	1.55	1.79	-1.09	68	-41	2.47
Autumn	9	1.49	1.01	0.89	-0.48	59	-32	1.10
<b>Total</b>	41	1.68	1.01	1.19	-0.67	71	-40	1.67

1339 <sup>a</sup> Statistics are calculated for a specific site type during all four seasons

1340 <sup>b</sup> Statistics are calculated for a specific continent excluding the values from urban areas

1341 <sup>c</sup> Statistics are calculated for a specific season excluding the values from urban areas

1342

1343 **Table 6.** Statistical evaluation of EMAC fresh SOA against AMS SV-OOA in the  
 1344 Northern Hemisphere during 2001-2010.

1345

<b>Site Type<sup>a</sup></b>	<b>Number of datasets</b>	<b>Mean Observed</b> ( $\mu\text{g m}^{-3}$ )	<b>Mean Predicted</b> ( $\mu\text{g m}^{-3}$ )	<b>MAGE</b> ( $\mu\text{g m}^{-3}$ )	<b>MB</b> ( $\mu\text{g m}^{-3}$ )	<b>NME</b> (%)	<b>NMB</b> (%)	<b>RMSE</b> ( $\mu\text{g m}^{-3}$ )
Urban Downwind	8	0.81	0.64	0.41	-0.17	51	-21	0.76
Rural/Remote	33	1.03	0.70	0.64	-0.33	62	-32	0.85
<b>Continent<sup>b</sup></b>								
Europe	35	0.90	0.63	0.56	-0.27	62	-30	0.81
N. America	6	1.51	1.07	0.80	-0.44	53	-29	0.96
Asia	-	-	-	-	-	-	-	-
<b>Season<sup>c</sup></b>								
Winter	3	0.87	0.18	0.69	-0.69	79	-79	0.76
Spring	18	0.54	0.37	0.46	-0.17	86	-31	0.60
Summer	11	1.89	1.22	0.96	-0.67	51	-36	1.27
Autumn	9	0.83	0.86	0.39	0.03	47	4	0.52
<b>Total</b>	41	0.99	0.69	0.60	-0.30	60	-30	0.83

1346 <sup>a</sup> Statistics are calculated for a specific site type during all four seasons

1347 <sup>b</sup> Statistics are calculated for a specific continent excluding the values from urban areas

1348 <sup>c</sup> Statistics are calculated for a specific season excluding the values from urban areas

1349

1350

1351

1352

1353

1354

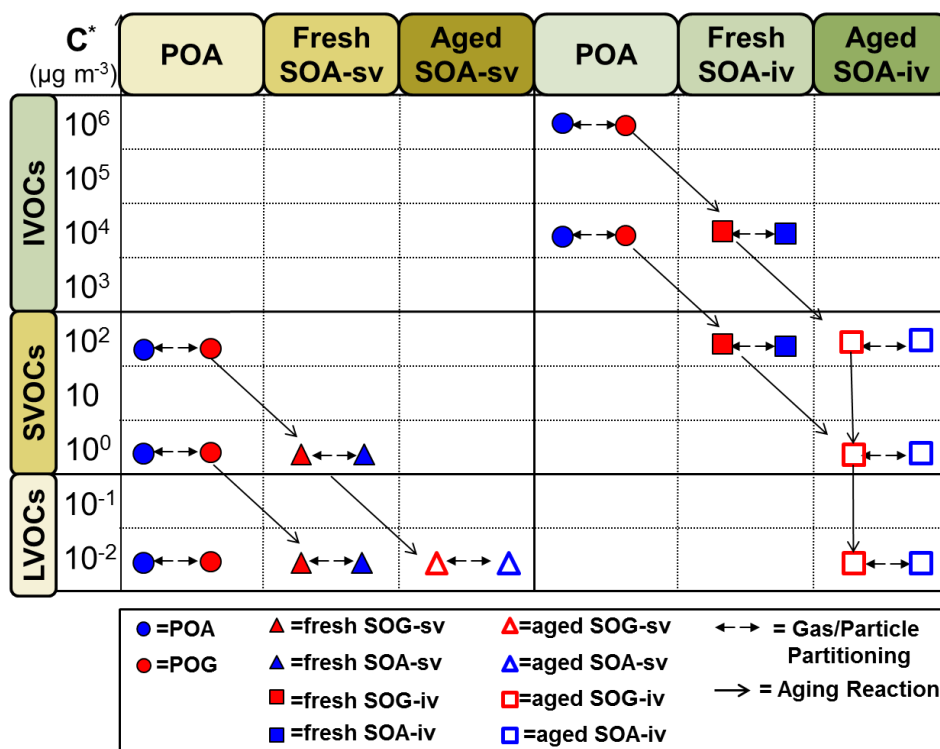
1355

1356

1357

1358

1359



1360

1361

1362 **Figure 1:** Schematic of the VBS resolution and the formation of SOA from SVOC

1363 and IVOC emissions. Red indicates the vapor phase and blue the particulate phase.

1364 The circles represent primary organic material that can be emitted either in the gas or

1365 in the aerosol phase. Filled triangles and squares indicate the formation of SOA from

1366 SVOCs and IVOCs, respectively, by fuel combustion and biomass burning sources

1367 from the first oxidation step (fresh SOA). Open triangles and squares represent SOA

1368 formed in additional oxidation steps (aged SOA) from SVOCs and IVOCs by the

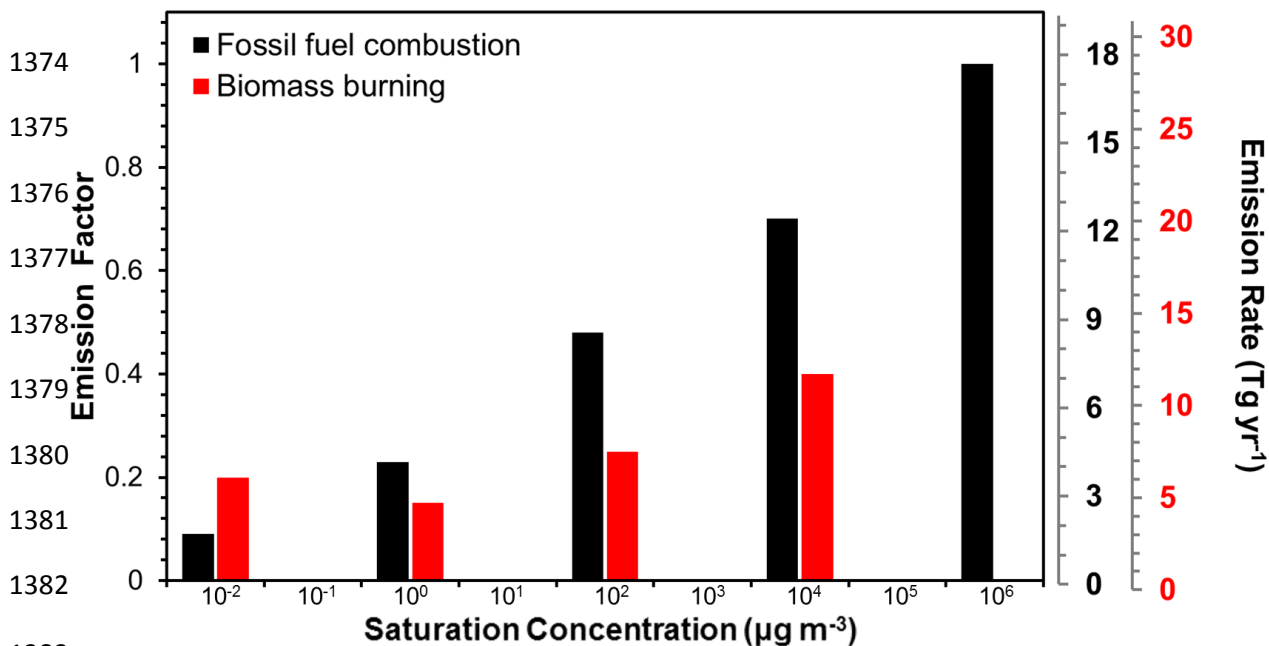
1369 same sources. The partitioning processes, the aging reactions of the organic

1370 compounds, and the names of the species used to track all compounds are also shown.

1371

1372

1373



1383

1384 **Figure 2.** Volatility distribution for fuel combustion (in black) and  
1385 biomass burning (in red) organic emissions. The emission factors for  
1386 fuel combustion emissions are derived from Robinson et al. (2007)  
1387 while for biomass burning POA emissions are from May et al. (2013)  
1388 (shown in the primary y-axis). The corresponding emission rates are  
1389 also shown in the secondary y-axis.

1390

1391

1392

1393

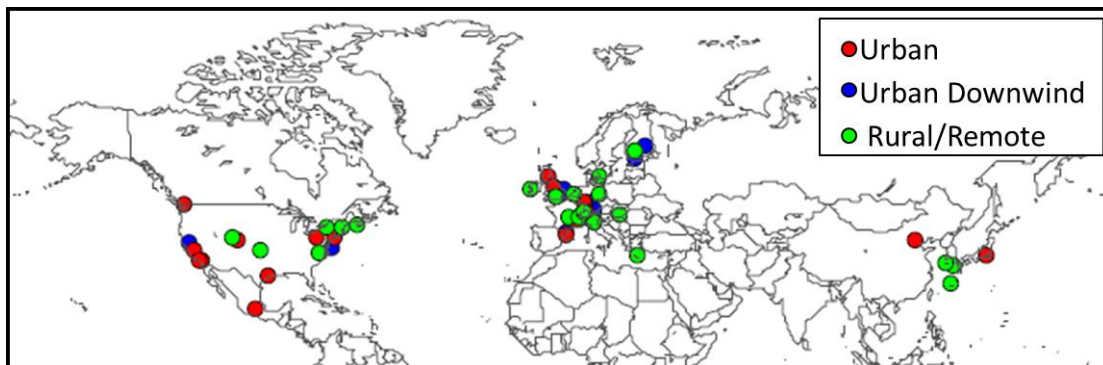
1394

1395

1396

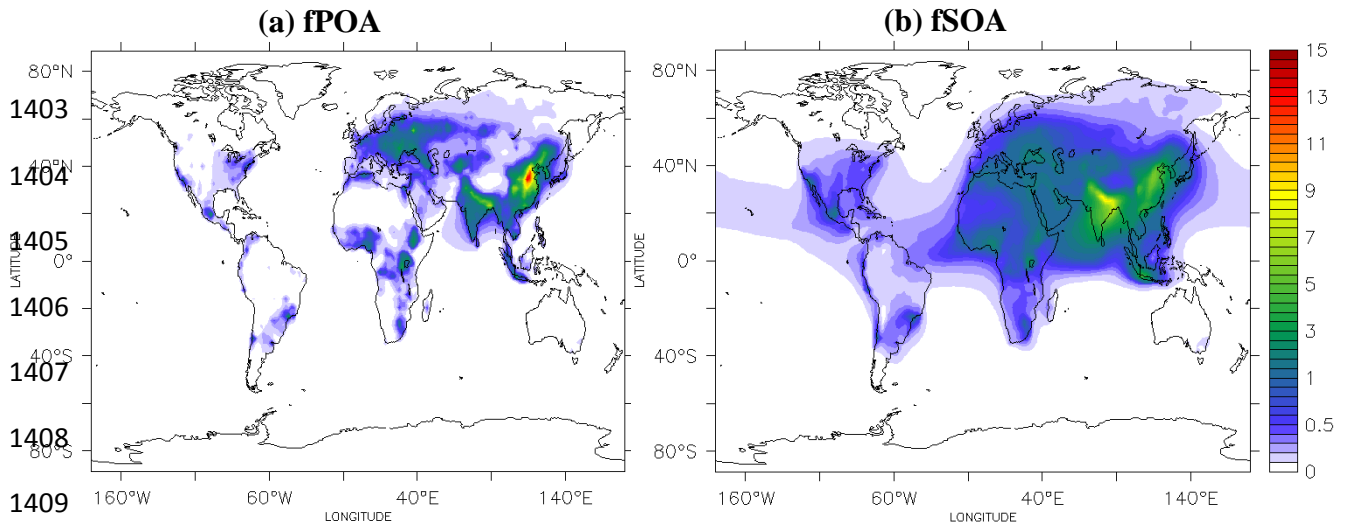
1397

1398



1399 **Figure 3:** Location of the field measurement campaigns used for evaluating the model  
1400 during 2001-2010. Urban, urban downwind and rural/remote areas are represented by  
1401 red, blue, and green colors respectively.

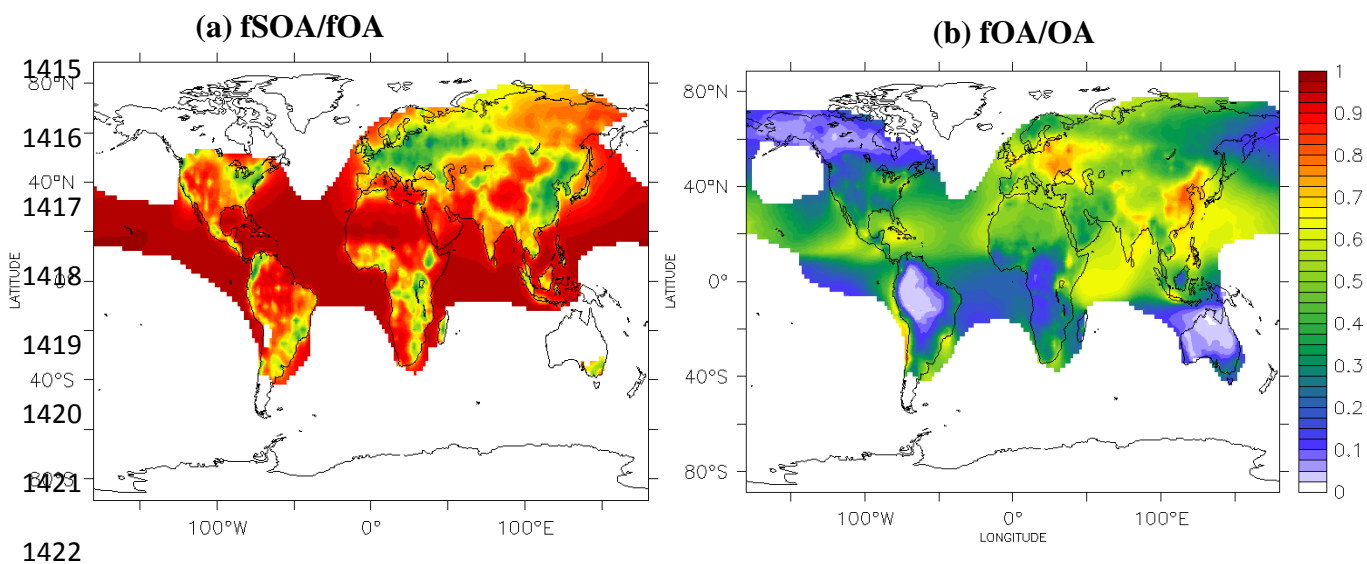
1402



1410

1411 **Figure 4:** Predicted average surface concentrations (in  $\mu\text{g m}^{-3}$ ) of: (a) POA from fuel  
 1412 combustion sources (fPOA) and (b) SOA from the oxidation of SVOCs and IVOCs  
 1413 from fuel combustion sources (fSOA) during the years 2001-2010.

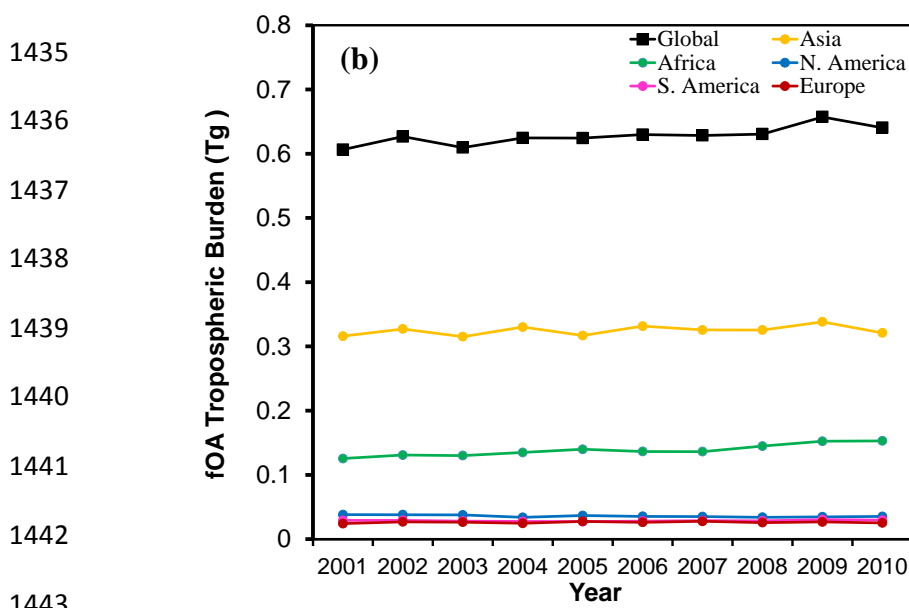
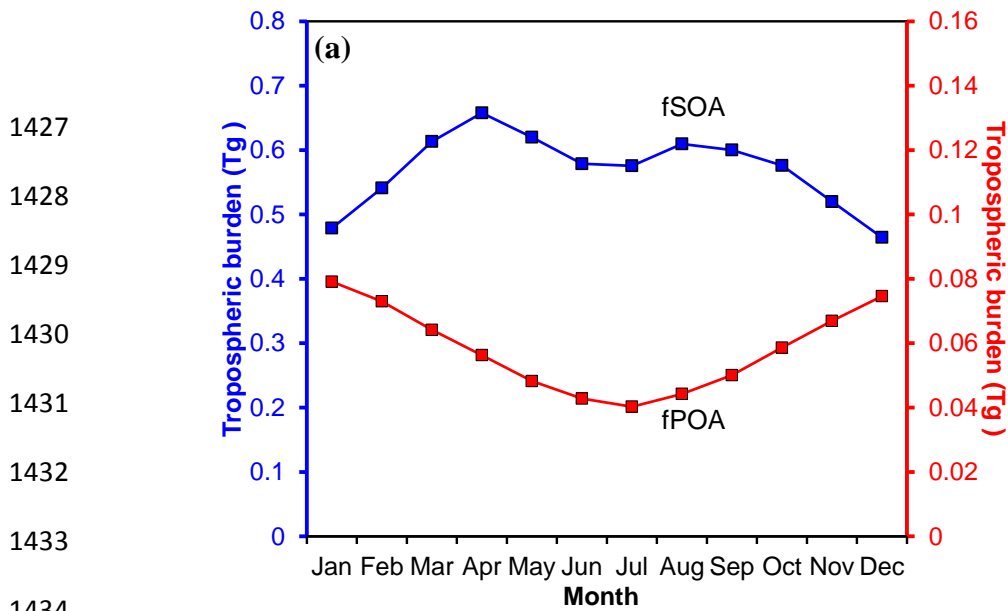
1414



1422

1423 **Figure 5:** Predicted ratio of (a) fuel combustion SOA (fSOA) to total fuel combustion  
 1424 OA (sum of fPOA and fSOA) and (b) fuel combustion OA to total OA (sum of fOA,  
 1425 bbOA, aSOA, and bSOA) during the years 2001-2010.

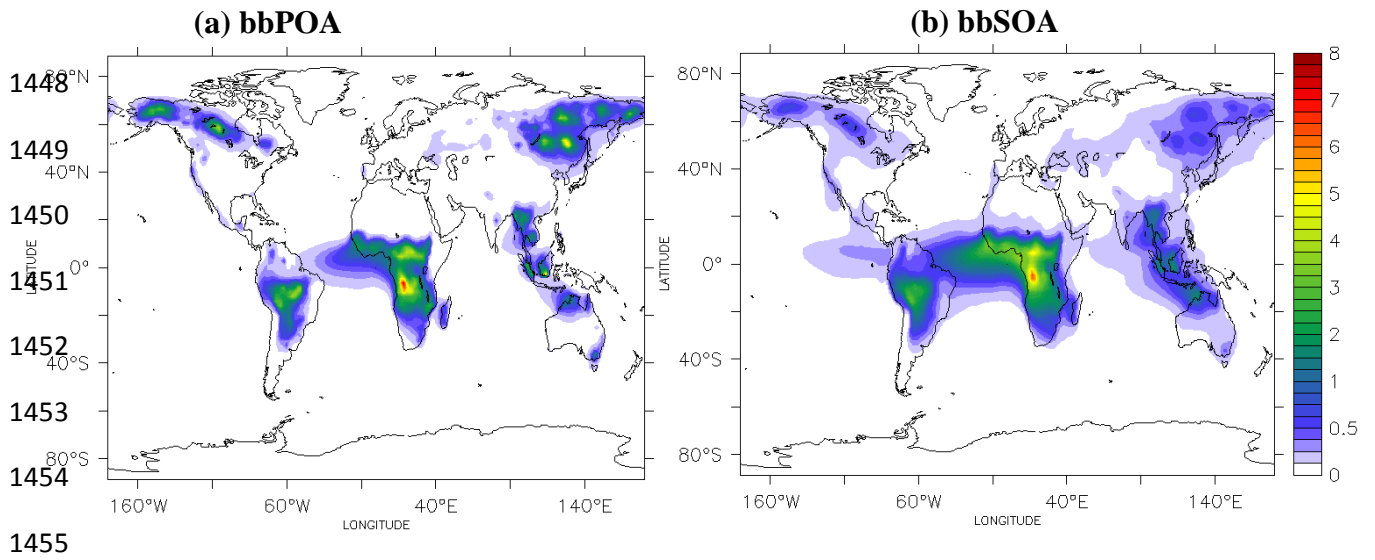
1426



1444 **Figure 6:** (a) Average predicted tropospheric burden (Tg) of fSOA (in blue, primary y-  
 1445 axis) and fPOA (in red, secondary y-axis) and (b) annually averaged tropospheric  
 1446 burden of total fuel combustion OA (fOA) during 2001-2010.

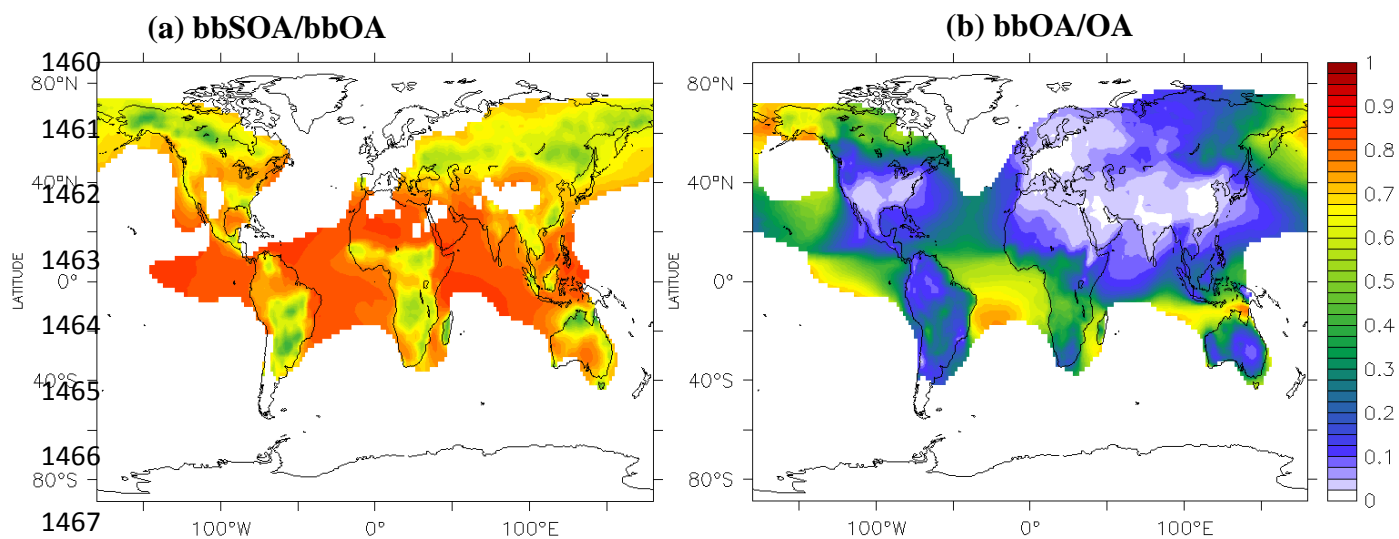
1447





1456 **Figure 7:** Predicted average surface concentrations (in  $\mu\text{g m}^{-3}$ ) of: **(a)** POA from  
 1457 biomass burning sources (bbPOA) and **(b)** SOA from the oxidation of SVOCs and  
 1458 IVOCs from biomass burning sources (bbSOA) during the years 2001-2010.

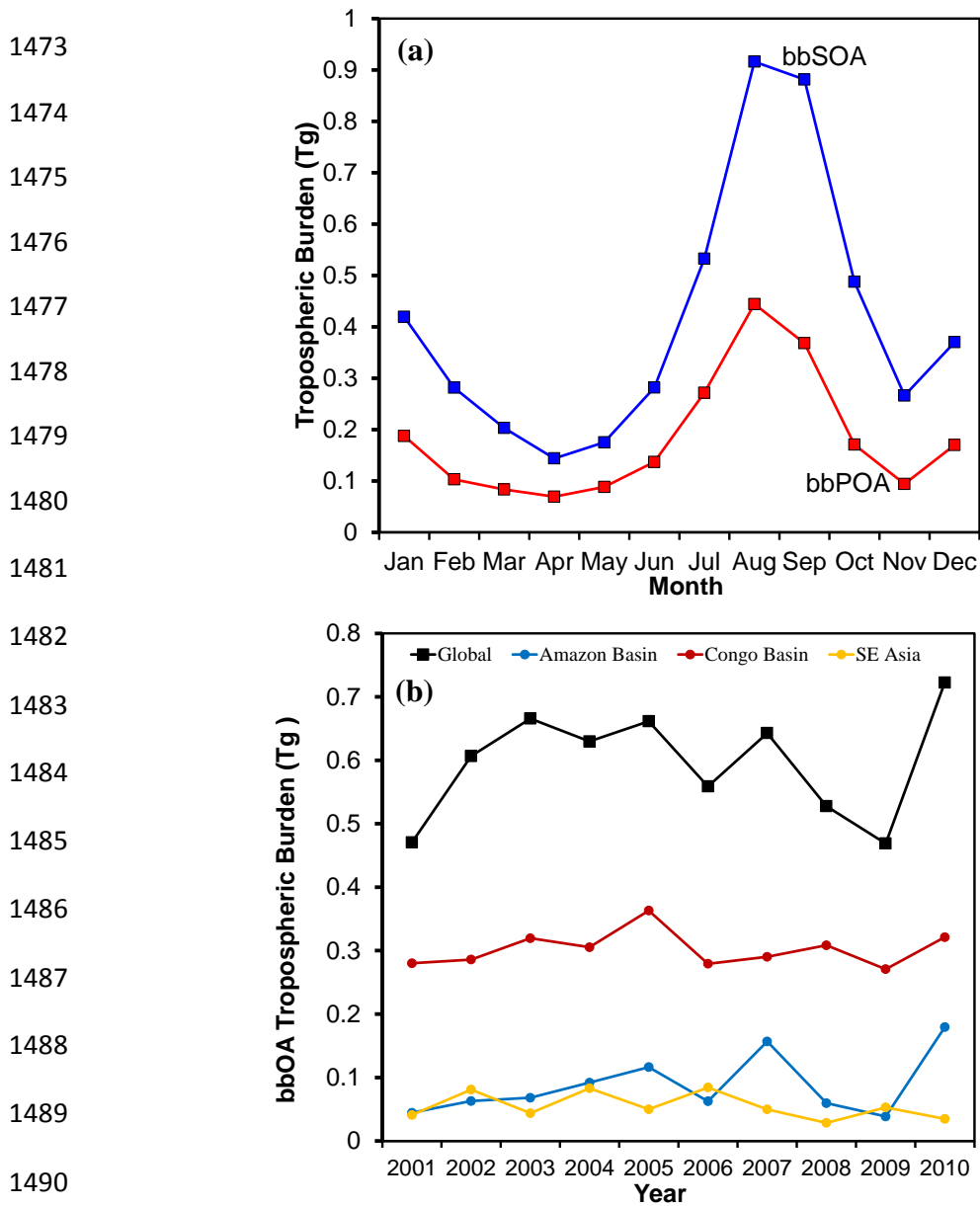
1459



1468

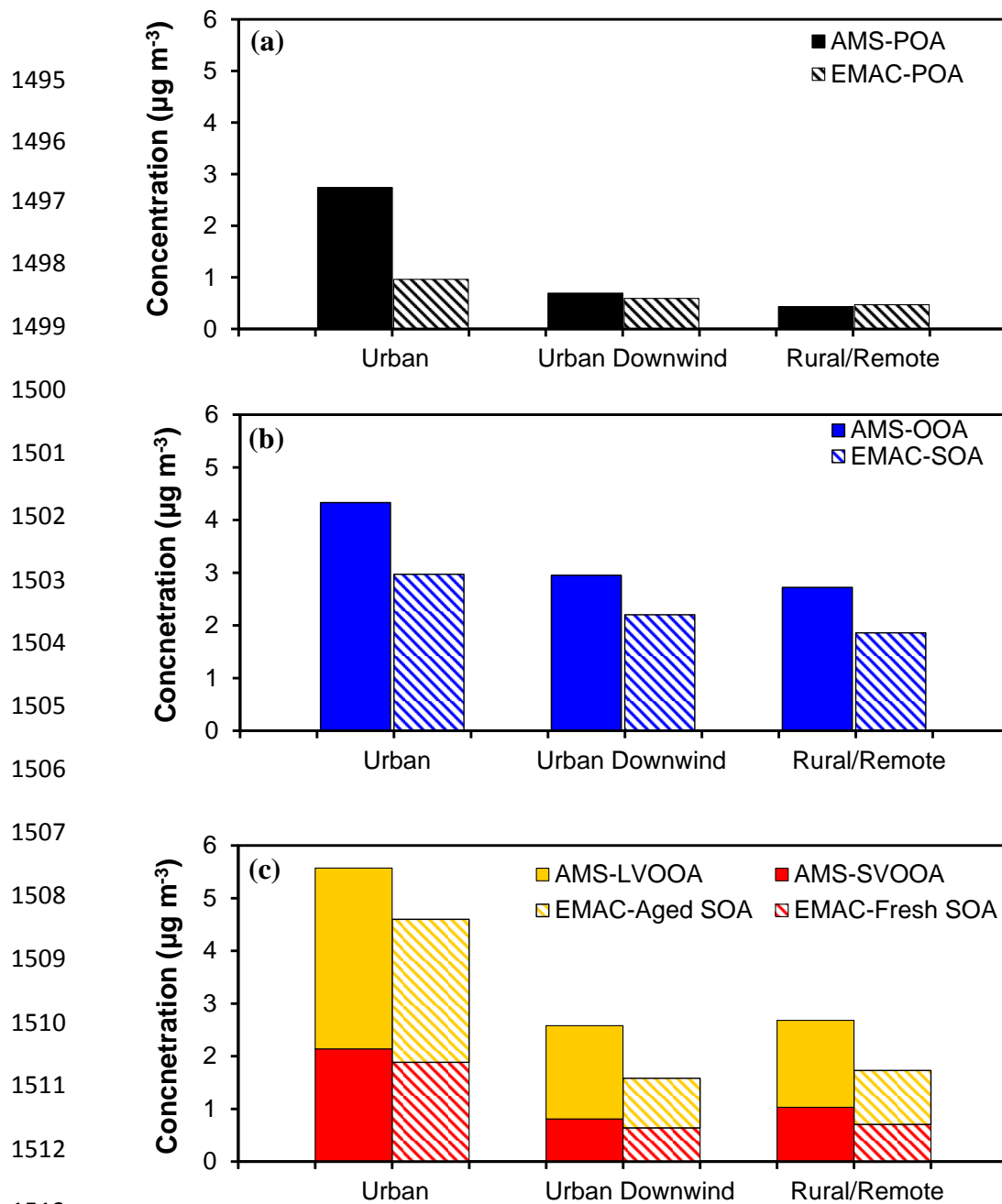
1469 **Figure 8:** Predicted ratio of (a) biomass burning SOA (bbSOA) to total biomass  
 1470 burning OA (sum of bbPOA and bbSOA) and (b) biomass burning OA to total OA  
 1471 (sum of fOA, bbOA, aSOA, and bSOA) during the years 2001-2010.

1472



1491 **Figure 9:** (a) Monthly averaged predicted tropospheric burden (Tg) of bbSOA (in  
 1492 blue) and bbPOA (in red) and (b) Annual average tropospheric burden of total  
 1493 biomass burning OA (bbOA) during 2001-2010.

1494



1514 **Figure 10:** Comparison of average (a) EMAC predicted POA to AMS-POA (sum of  
 1515 AMS-HOA and AMS-BBOA) (b) EMAC predicted SOA to AMS-OOA, and, (c)  
 1516 EMAC predicted fresh and aged SOA to AMS-SVOOA and AMS-LVOOA from 84  
 1517 data sets over urban, urban downwind and rural/remote areas during 2001-2010.

1518

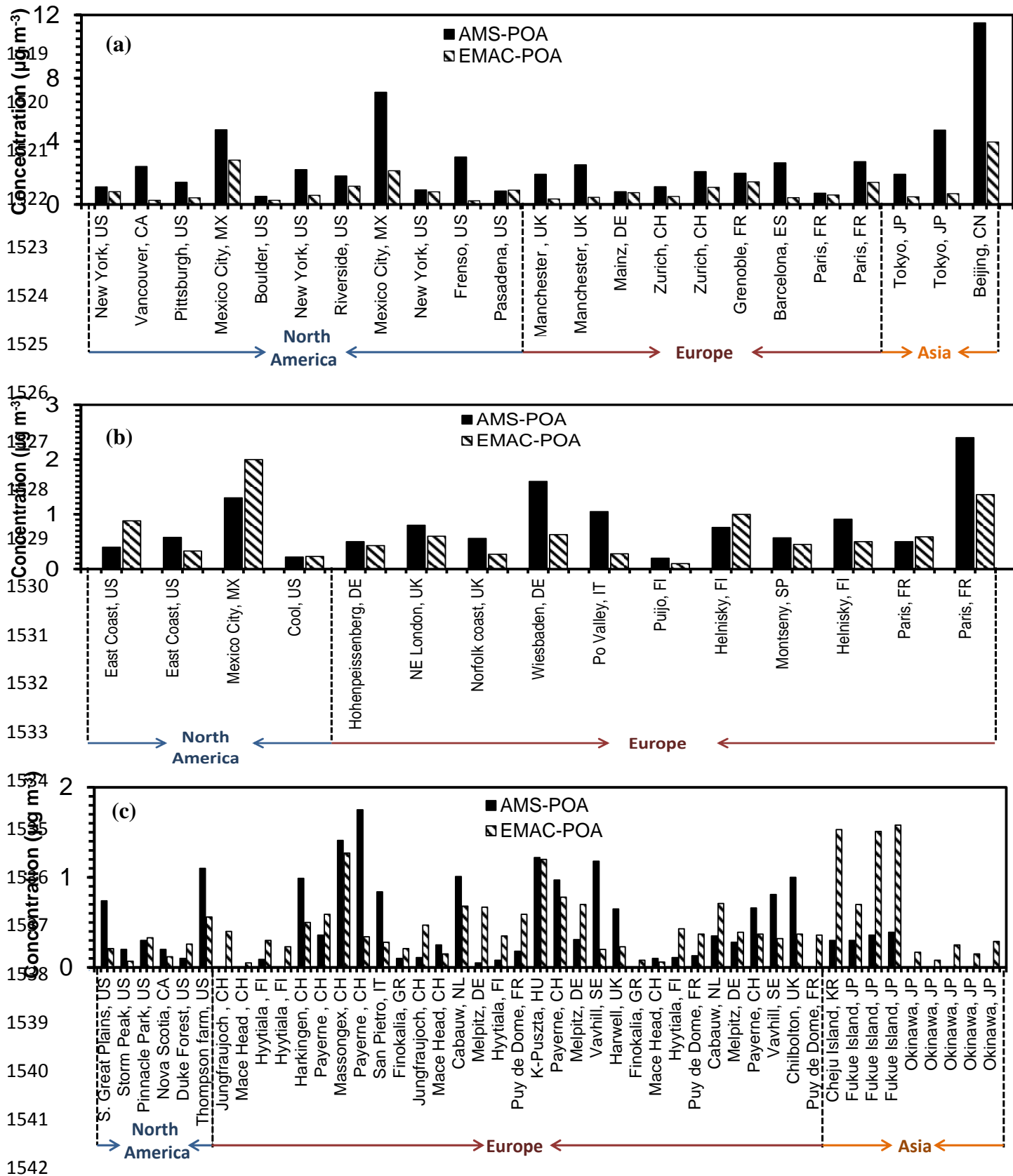
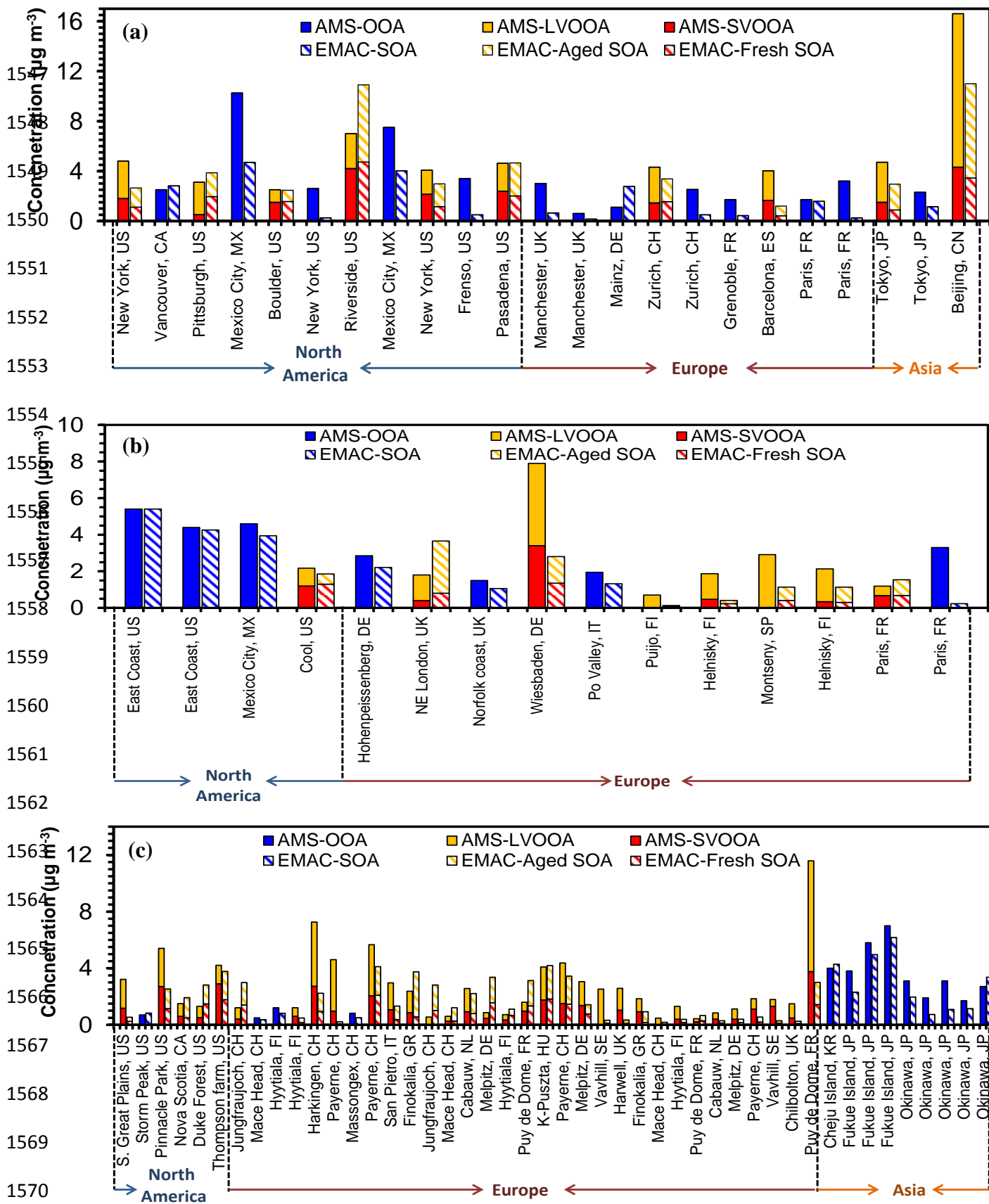


**Figure 11:** Comparison of EMAC POA (sum of fPOA and bbPOA) to AMS POA (sum of HOA and BBOA) from 84 data sets worldwide over (a) urban, (b) urban downwind and (c) rural/remote areas during 2001-2010.

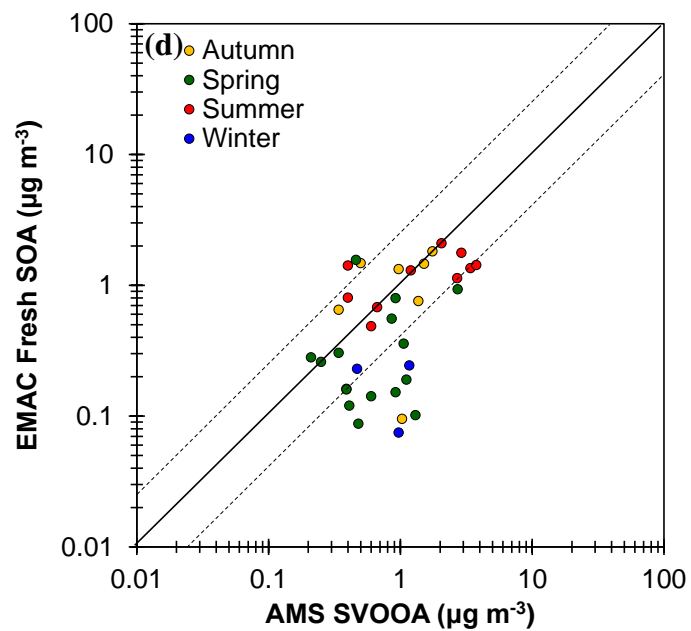
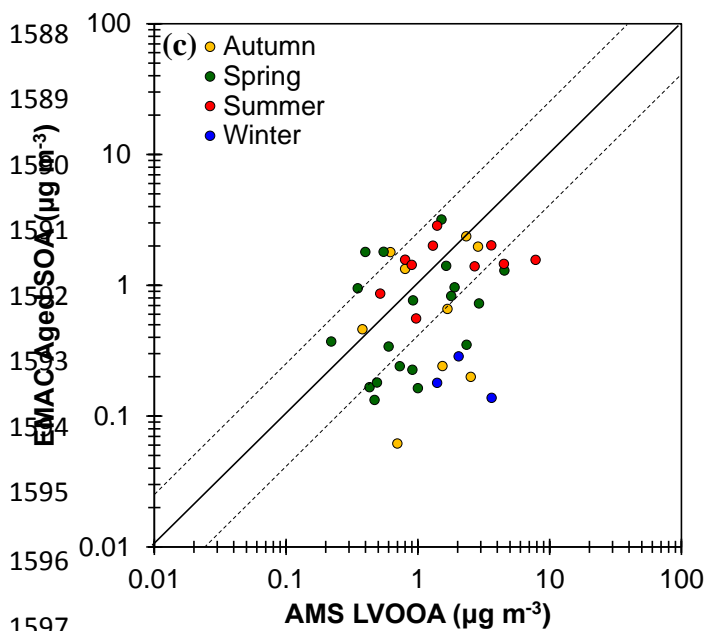
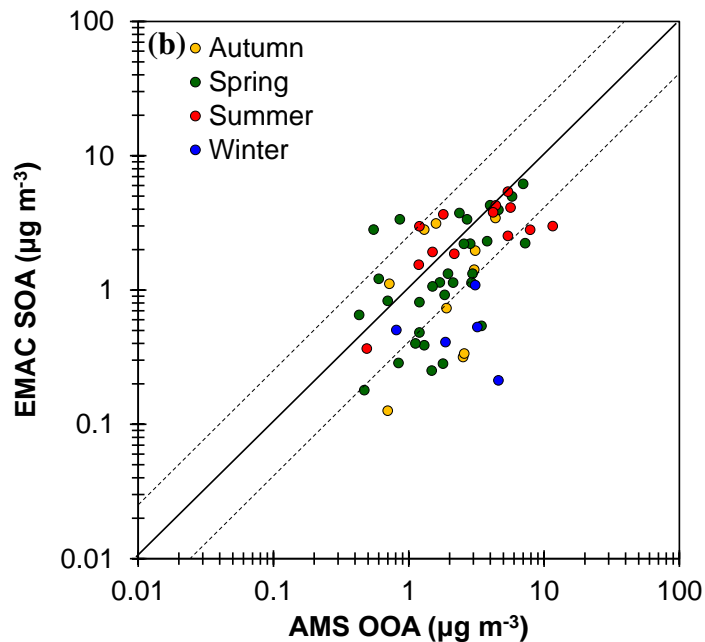
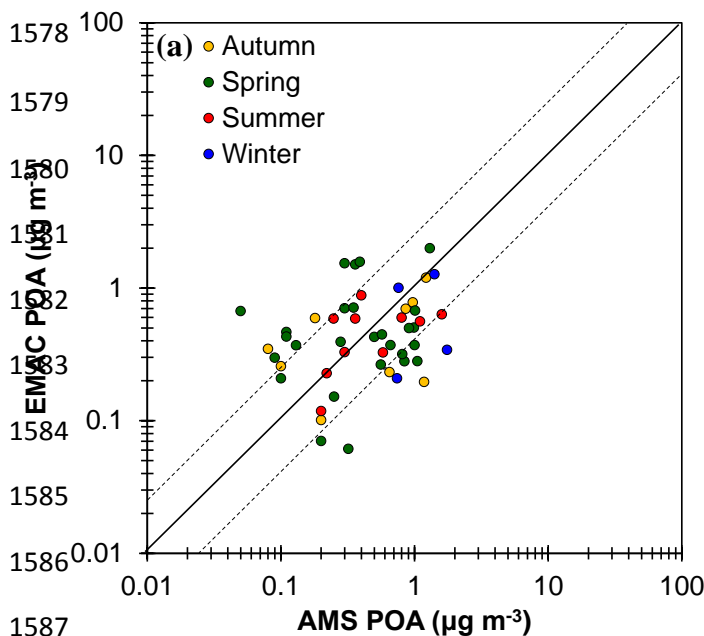


1571 **Figure 12:** Comparison of EMAC SOA (fresh SOA and aged SOA) to AMS OOA  
 1572 (SV-OOA and LV-OOA) from 84 data sets worldwide over (a) urban, (b) urban  
 1573 downwind and (c) rural/remote areas during 2001-2010.

1575

1576

1577



1597

1598

1599 **Figure 13:** Scatterplots comparing model results to AMS for: (a) POA, (b) OOA, (c)  
1600 LV-OOA, and (d) SV-OOA concentrations (in  $\mu\text{g m}^{-3}$ ) in the Northern Hemisphere  
1601 during 2001-2010. Each point represents the data set average value and is colored  
1602 based on the season of the field campaign. Also shown are the 1:1, 2:1, and 1:2 lines.

1603

1604

1605

1606

1607

1608

1609

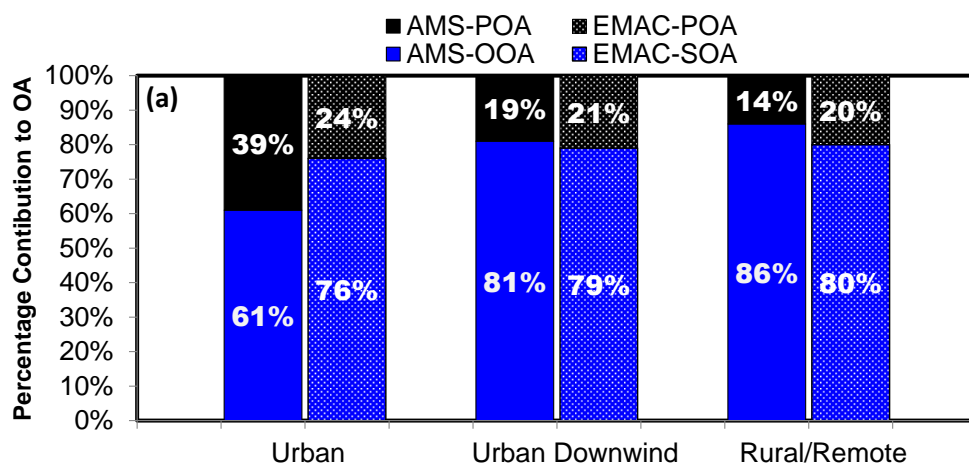
1610

1611

1612

1613

1614



1615

1616

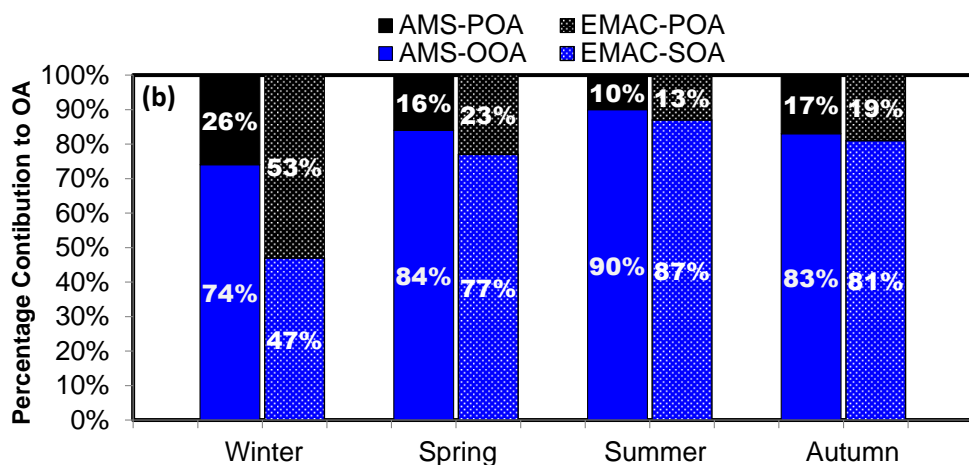
1617

1618

1619

1620

1621



1622 **Figure 14:** (a) Spatial and (b) seasonal composition of total OA mass calculated from  
1623 EMAC and AMS results in the Northern Hemisphere during 2001-2010.

1624



1625  
 1626  
 1627  
 1628  
 1629  
 1630  
 1631  
 1632  
 1633  
 1634  
 1635  
 1636  
 1637  
 1638  
 1639  
 1640  
 1641  
 1642  
 1643  
 1644  
 1645  
 1646  
 1647  
 1648

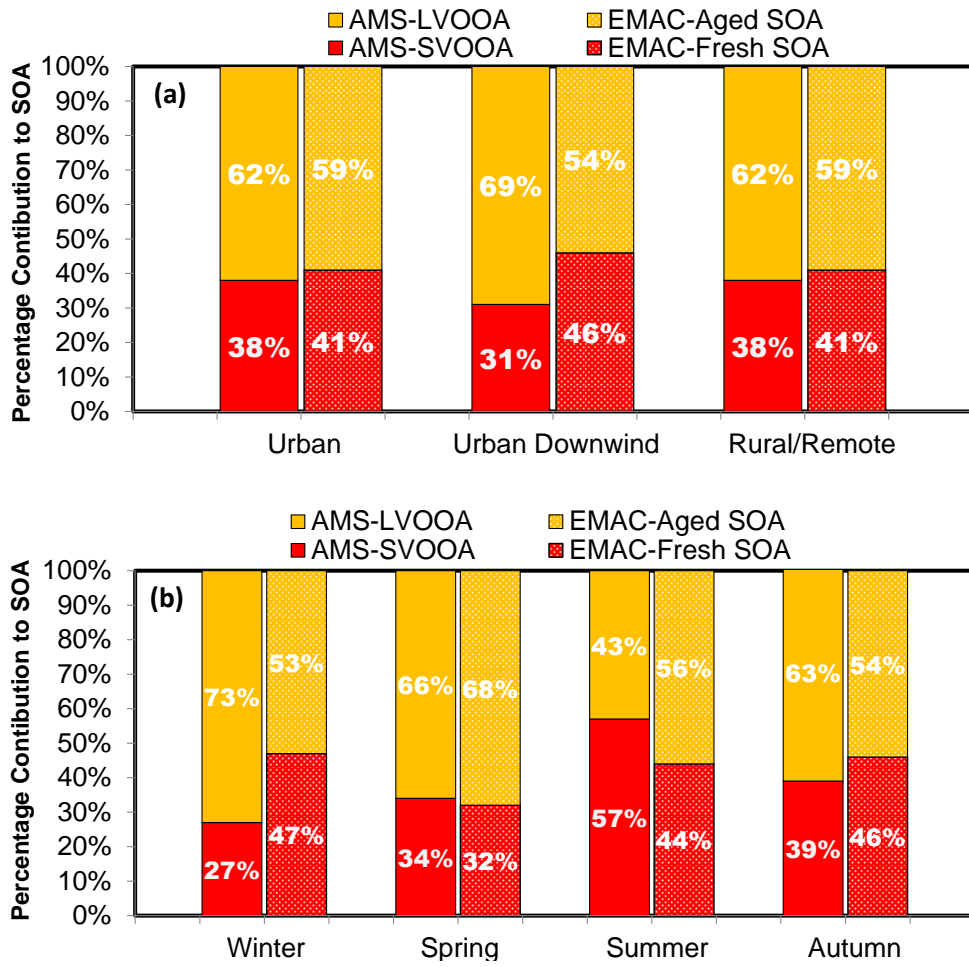


**Figure 15:** (a) Spatial and (b) seasonal composition of SOA and OOA mass calculated from EMAC and AMS results, respectively, in the Northern Hemisphere during 2001-2010.